FIRST PRINCIPLES CALCULATION OF $LaAlO_3/SrTiO_3$ INTERFACIAL TRANSPORT PROPERTIES

LO WING CHONG

M.Phil

The Hong Kong Polytechnic University

2014

THE HONG KONG POLYTECHNIC UNIVERSITY

THE DEPARTMENT OF APPLIED PHYSICS

First Principles Calculation of $LaAlO_3/SrTiO_3$ Interfacial Transport Properties

Lo Wing Chong

A thesis submitted in partial fulfillment of the requirements

for the degree of Master of Philosophy

JUNE 2013

CERTIFICATE OF ORIGINALITY

I hereby declare that this thesis is my own work and that, to the best of my knowledge and belief, it reproduces no material previously published or written nor material which has been accepted for the award of any other degree or diploma, except where due acknowledgement has been made in the text.

_____ (Signature)

Lo Wing Chong (Name of candidate)

ABSTRACT

Since 2004 many interesting phenomena have been discovered at the high-mobility two dimensional electron gas (2DEG) between two band insulators $LaAlO_3$ (LAO) and $SrTiO_3$ (STO). The model of polar catastrophe and electronic reconstruction successfully explains formation of the LAO/STO 2DEG. However, the research of LAO/STO is now turning from intrinsic LAO/STO system into other directions such as surface modulation by polar liquid that may lead to novel properties and applications. The objective of my thesis is to provide theoretical understanding on the mechanism behind these new phenomena.

Project density of states (DOS) and carrier density calculation results reveal that, the conduction properties at LAO/STO interface can be greatly influenced by water molecules adsorbed on the LAO surface. Due to the strong polar field produced by H_2O molecules, the surface electronic structure can be affected by just a few H_2O layers. The carrier density of the 2DEG interface can be greatly increased by a few layers of H_2O molecules. Work function of LAO/STO heterostructure will also change significantly, and this may explain the rectified I-V curve for the conduction through the polar molecule covered part and the uncovered part of LAO/STO.

Recently, there are also some studies on different oriented LAO/STO interface. (110) and (111) LAO/STO transport properties and the results may challenge the polar catastrophe model in the formation of 2DEG. Based on the calculations reported in this thesis, it is unlikely to obtain polar catastrophe at both (110) and (111) LAO/STO

interfaces. At the (110) LAO/STO, the conduction electrons should be localized along [1 -1 0], but transport easily along [0 0 1]. While at the (111) LAO/STO interface, electrons may be localized in all plane directions. Doping effects are also studied. The results of n-type doping (110) and (111) interfaces reveal that the electrons, unlike those at (001) interface, are not confined strongly at interfaces, and the results of p-type doping show that holes spread over LAO and STO layers.

SCHOLARLY ACTIVITIES

Journal Papers

1. W.C. Lo, Kit Au, N. Y. Chan, Haitao Huang, Chi-Hang. Lam *and* J. Y. Dai "First principles study of transport properties of $LaAlO_3/SrTiO_3$ heterostructure with water adsorbates", Solid State Communications, vol. 24, pp. 2598-2062, 2013

2. W.C. Lo, Kit Au, N. Y. Chan, Haitao Huang *and* J. Y. Dai "First principles study of (110)-oriented $LaAlO_3/SrTiO_3$ interface", under preparation

3. W.C. Lo, Kit Au, N. Y. Chan, Haitao Huang *and* J. Y. Dai "First principles study of (111)-oriented $LaAlO_3/SrTiO_3$ interface", under preparation

Conference presentation

1. W.C. Lo, K. Au, N.Y. Chan, H.T. Huang, C.H. Lam and J.Y. Dai "Investigation of H2O Molecule Adsorbed LaAlO3/SrTiO3 Heterointerface by First Principles" in European Materials Research Society (EMS) 2013Spring Meeting

ACKNOWLEDGEMENTS

I would like to express my gratitude to my supervisor Dr J.Y. Dai for his supervision and support with patience throughout my M.Phil study. He gives me a large degree of freedom, even when my research was stuck by difficulties. I am so grateful for latitude he gave me.

I would like to specifically thank my co-supervisor Dr H. Huang for the valuable advices. I have learnt so much from him since I was under his supervision in final year project of my undergraduate study.

I want to thank Dr. C.H. Lam for discussion and suggestions he provided.

I thank Mr. K. Au, Mr. N. Y. Chan, Mr. K. W. Mak and Ms S. M. Ng for their help in these two years.

Finally, I give my appreciation to my parents for their endless love and care.

TABLE OF CONTENTS

LIST OF FIGURES

LIST OF TABLES

CHAPTER 1 INTRODUCTION

1.1 Background of Thesis

Epitaxial growth of oxide thin film in atomic scale is a rapidly developing area of materials science. The surface and interface of oxide thin films exhibit interesting physics and the extraordinary properties which may lead to valuable applications, such as memories, transistors and sensors.

In 2004, Ohtomo and Hwang discovered the high-mobility two dimensional electron gas (2DEG) arising from the (001) interface of two band insulators $LaAlO_3$ (LAO) and $SrTiO_3$ (STO) [1]. When LAO was epitaxially grown on TiO2-terminated STO, the interface became metallic conducting with LAO layer beyond a critical thickness of 4 unit cells. Electronic reconstruction was suggested to be responsible for compensation of polar discontinuity between polar LAO and nonpolar STO. Since then, the interfaces of polar / nonpolar oxides have been extensively studied experimentally and theoretically [2-14]. Many interesting properties at LAO/STO heterostructure, such as conductivity, superconductivity and magnetic ordering, have been reported [4, 10-15]. The interfacial transport properties are also affected by oxygen partial pressure during fabrication, indicating that oxygen vacancy should play an important role in the LAO/STO 2DEG [5-7]. However, the thin film of LAO on SrO-terminated STO remains insulating [1]. In this thesis, the LAO/STO refers to the LaO/TiO_2-terminated LAO/STO heterostructure if there is no mention.

Controllable transport properties were also reported and non-linear I-V relations were obtained under electric field or magnetic field [2-4]. The band gap was proposed to vary with the number of LAO layers below critical thickness in ab initio study in supplement of ref [2]. Moreover, conducting state was shown to be sensitive to surface charge state and hysteresis loop was obtained [16, 17]. These results may lead to applications in electronic devices.

The interfacial transport properties were found to be affected by capping layers [18, 19], and surface adsorbates [20-23]. For example, it was found in experiments that the concentration of conduction electrons at interface changes with adsorbates on LAO surface [21, 22] where several kinds of polar liquids including water were added; while theoretical study [23] shows that hydrogen atoms on LAO/STO provide electrons to the LAO/STO interface. Au *et al.* discovered the rectified I-V curves with water on LAO/STO heterostructure and it was suggested that Schottky junctions form between areas covered by polar liquids and areas without polar liquids. [22] It should be helpful to the development of novel sensors if the physics behind can be further understood. To the best of my knowledge, no theoretical study has been reported for the effect of polar liquids on the interface transport. In this thesis work, first principles study has therefore been applied on the system of LAO/STO heterostructure with water molecules on the surface.

Most recently, 2DEGs were reported to appear in other oxide systems, also including (001) STO surface, amorphous oxides on STO, and (110) and (111) LAO/STO interfaces.[24, 25] It is unexpected to obtain metallic interface in amorphous

oxides STO heterostructure or (110) LAO/STO interface, since these systems should not have significant polar discontinuity as (001) LAO/STO. The (110) and (111) LAO/STO heterostructures need to be investigated theoretically, since the transport mechanism in these systems remains unknown.

1.2 Two-Dimensional Electron Gas (2DEG) at $LaAlO_3/SrTiO_3$ Interface

1.2.1 Introduction of 2DEG

Two-Dimensional Electron Gas (2DEG) is a gas of electrons that is confined in one dimension but is free to move in the other two dimensions. It was firstly discovered in interfaces of semiconducting materials, such as ZnO/MgZnO, Ge/GaAs and GaAs/AlGaAs [26-28]. Since the 2DEG is confined in one dimension, it leads to a quantum well and exhibit some quantum effects such as Quantum Hall Effect (QHE) and weak antilocalization [8, 28-30].

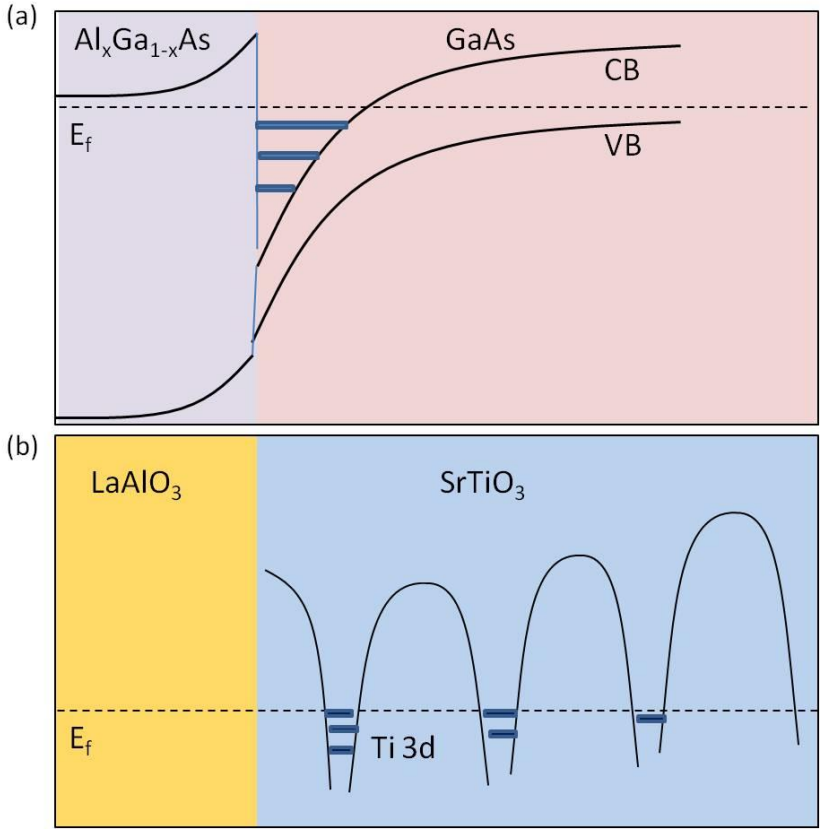

Figure 1-1 Comparison of the 2DEG systems at (a) interface of semiconductors, and (b) LAO/STO interface [8, 31]

However, some properties are quite different between 2DEG in semiconductors and those in $LaAlO_3$ (LAO)/ $SrTiO_3$ (STO) heterointerface indicated by Mannhart and Schlom [8]. The 2DEG at (001) LAO/STO interface is regarded as a strongly correlated electronic system. Theoretical studies suggest that conduction electrons occupy Ti 3d orbitals, so the electron gas distributes separately in layers of TiO_2 parallel to the (001) interface of LAO/STO that form a structure of a set of quantum wells as shown in Figure 1-1. Some researchers even suggested to call the system to be Two-Dimensional Electron Liquid (2DEL) [8, 18, 31-33] because of its correlated nature.

1.2.2 Perovskite Oxides

The heterostructure of $LaAlO_3/SrTiO_3$ is formed by two perovskite oxides $LaAlO_3$ and SrTiO3. Perovskite oxides have the chemical formula ABO_3, where A and B are two different cations. Perovskite oxides may exhibit various properties such as piezoelectrics, ferroelectrics, and multi-ferroics.

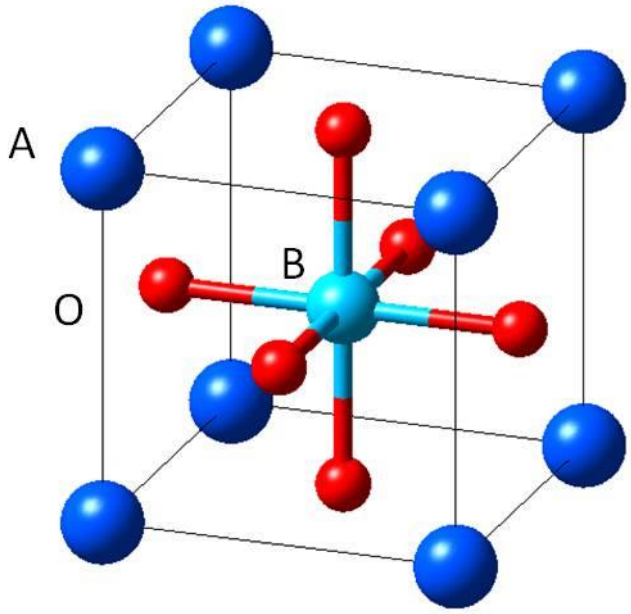

Figure 1-2 A unit cell of a cubic perovskite ABO_3, and A : deep blue ball at corners; B: light blue ball in the middle; O: red balls at the center of faces.

In Figure 1-2, the high-temperature parent structure of perovskites (ABO_3) is cubic, like $SrTiO_3$ at room temperature, and $LaAlO_3$ and $BaTiO_3$ at high temperature. In this structure, cation A is located at the corner; while B is located at the center; and O at the face centers of the cube. However, phase transitions of perovskite oxides usually occur at low temperature and the structure would be distorted from cubic. $LaAlO_3$ has

rhombohedral structure at room temperature, but the structure can still be treated as pseudo-cubic [34, 35]. $BaTiO_3$ exhibits a series of phase changes from cubic to tetragonal, orthorhombic and rhombohedral phase, when the temperature is reduced [36]. In $BaTiO_3$ Ti shifts from center to [001], [110] and [111] direction corresponding to tetragonal, orthorhombic and rhombodedral structures. Lattice of $SrTiO_3$ becomes tetragonal and TiO_6 octahedra rotates when temperature is below 105K [37, 38]. It is believed that such a rotation of BO_6 octahedra prevents the B atom to shift from center to give rise to ferroelectricity [37, 38].

$SrTiO_3$ has an indirect band gap of 3.2 eV and $LaAlO_3$ has a wide band gap of 5.6 eV. Many perovskite oxides are insulators, like $SrTiO_3$ and $LaAlO_3$. There are also metallic perovskite oxides, such as $SrRuO_3$. The electrical conductivity of perovskite oxides however can be varied by doping or introducing oxygen vacancies. For example, Nb-doping or oxygen vacancies produce n-type conductivity in $SrTiO_3$, while the Sc-doped $SrTiO_3$ shows p-type conductivity [39]. Nb-doped $SrTiO_3$ and $SrTiO_3$ with oxygen vacancies exhibit superconductivity at low temperature [40].

1.2.3 Mechanism of the Formation of 2DEG

There are several mechanisms suggested to explain the formation of two-dimensional electron gas (2DEG) at LAO/STO (001) interface: polar catastrophe, oxygen vacancies, and interface mixing [6, 7, 9].

Polar discontinuity occurs at the interface of polar $LaAlO_3$ (LAO) and non-polar $SrTiO_3$ (STO). Thin film of perovskite oxides ABO_3 along [001] can be regarded as a stacking of atomic layers of alternating AO and BO_2 planes. In STO, the planes SrO and TiO_2 are neutral in the ionic limit, but the planes LaO and AlO_2 in LAO are positively and negatively charged alternatively. When LAO is epitaxially grown on STO, it forms a capacitor-like structure at LAO, and its potential increases proportional to the thickness of LAO. Polar-catastrophe appears with thick LAO layer, while electronic reconstruction appears to compensate the polar discontinuity. The polar-catastrophe model has been confirmed by theoretical studies showing that the polarization of LAO causes the electronic state at LAO to become less stable and electrons may be transferred to interface [41-45] as shown in Figure 1-3. This fact suggests that electronic reconstruction at the interface and consequently the electron gas exists mostly at the interface. Another important factor is the thickness. As shown in Figure 1-3 (b), to turn the LAO/STO interface into metallic conducting, the LAO thin film must be more than the critical thickness (4 unit cells). Otherwise, the thin film would behave insulating or semi-conducting [2, 46], as show in Figure 1-3 (a).

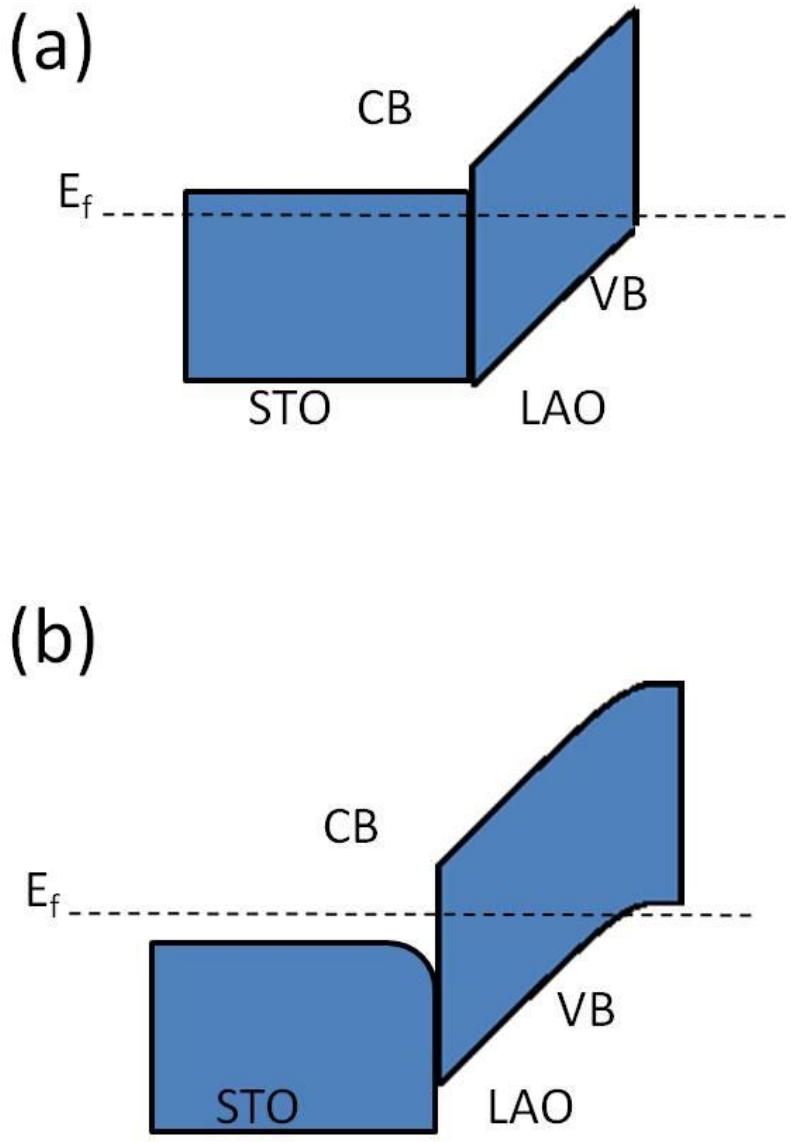

Figure 1-3 Sketch of the band structures of LAO/STO interface along normal direction that the LAO layer is, (a) less than the critical thickness, and (b) more than the critical thickness. The band structure can be obtained from layer-DOS [47]

Oxygen vacancies should also play a role in the transport properties of the heterostructure of LAO/STO interface. Oxygen vacancies may be formed at the LAO layer and the interfacial transport properties may be varied as introduced in section 1.2.2 of this thesis showing that oxygen vacancy provides more n-type carriers (electrons). At low temperature, it might also lead to magnetism and superconductivity

at the interface [11, 12, 15]. However the reports are controversial [11, 15] and the cause of the magnetism and superconductivity of the interface remains unclear.

Interface mixing may also reduce the energy at interface and metallic $La_{(1-x)}Sr_xTiO_3$ may be formed between LAO and STO due to cationic mixing [48]. Measurements such as scanning transmission electron microscopy/electron energy loss spectroscopy (STEM/EELS) and Shubnikov–de Haas (SdH) oscillations [9] revealed that the LAO/STO interface behaves like $La_{(1-x)}Sr_xTiO_3$.

All of the three mechanisms mentioned above are possible to occur at LAO/STO heterointerface. Oxygen vacancies may be related to the magnetism and superconductivity. Polar-catastrophe model can directly explain the critical thickness of LAO; this is also confirmed by first principles calculations [31, 41, 42, 49]. Chamber [9] however suggested that the interface is not atomically sharp between LAO and STO. Interface mixing and defects may also occur at the interface. Density functional theory (DFT) calculation underestimates the band gap, and therefore, the critical thickness should increase to 5 or 6 unit cells of LAO under the model of polar catastrophe with perfect interface if band gap is adjusted to a correct value.

1.2.4 Transport Properties of 2DEG at $LaAlO_3/SrTiO_3$

Though both $LaAlO_3$ and $SrTiO_3$ are insulators, metal-insulator transition occurs in $LaAlO_3/SrTiO_3$ heterostructure when the interface termination is LaO/TiO_2 and the thickness of LAO is over 4 unit cells. The interface remains insulating with AlO_2/SrO

termination. The 2DEG at the LAO/STO interface has the Hall mobility about 10^3 $cm^2V^{-1}S^{-1}$, and the sheet carrier density is around 10^{13} cm^{-2}.

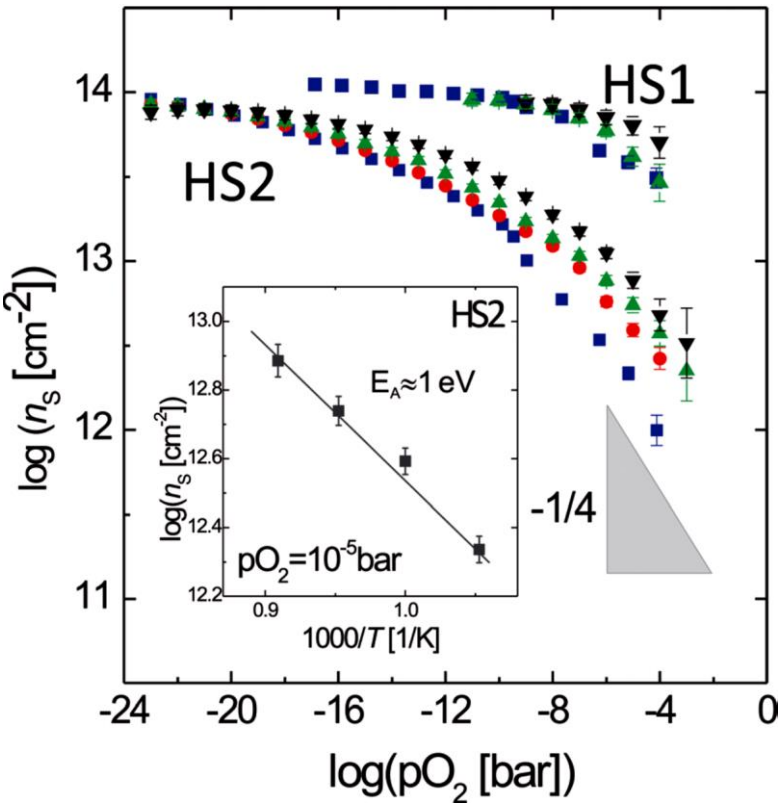

Figure 1-4 The sheet carrier density (n_s) at the LAO/STO-interface as a function of oxygen partial pressure (pO2) at various temperatures (950K (■), 1000K (●), 1050K (▲), and 1100K (▼)). HS1 corresponds to LAO/STO, HS2 to LAO/STO/LSAT. Inset: Arrhenius-plot of n_S at pO2=10^{-5} bar for HS2. Reprinted with permission from [5]. Copyright 2012, American Institute of Physics

Transport properties, including mobility and carrier density, depend on the condition of fabrication and annealing, such as oxygen partial pressure etc [5-7]. From Figure 1-4, sheet carrier density of the 2DEG decreases with ambient oxygen pressure at temperatures from 950 to 1100K. High oxygen pressure is believed to remove oxygen vacancies from the thin film, and Gunkel *et al.* [5]also suggested that it could increase

the cation vacancy concentration, such as Sr vacancies, at the interface. These may result in a decrease of sheet carrier density n_s as shown in Figure 1-4.

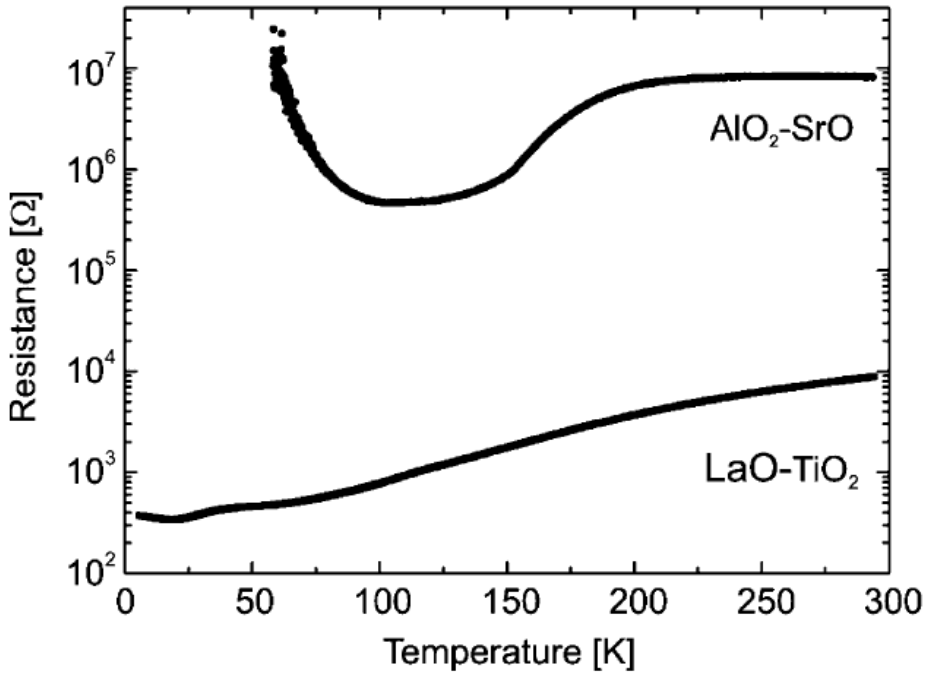

Figure 1-5 Temperature dependence of resistance of LAO/STO with AlO2/SrO and LaO/TiO_2 terminated interface. Reused with permission from [6]. Copyright © 2009 WILEY-VCH Verlag GmbH & Co. KGaA, Weinheim.

Temperature-dependent resistance of the LAO/STO with AlO_2/SrO and LaO/TiO_2 terminated interfaces is shown in Figure 1-5. LAO on a TiO_2-terminated STO surface behaves as metallic, but the LaO/SrO interface is insulating [6]. Superconductivity has also been discovered in LaO/TiO_2 terminated interface with a transition temperature around 200 mK [11-13, 15].

1.2.5 Surface Modulation of $LaAlO_3/SrTiO_3$ Heterostructure

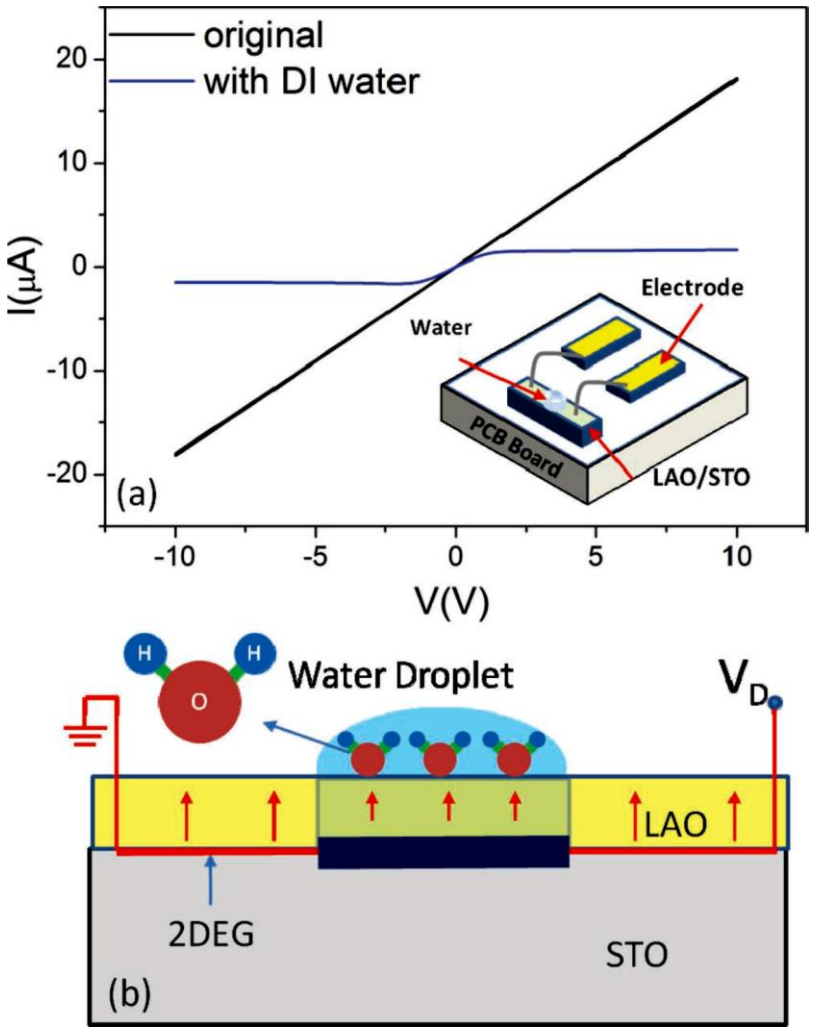

Figure 1-6 (a) I–V curves of the LAO/STO interface with and without water droplet on LAO surface. The inset is a schematic diagram showing the sensor structure. (b) Schematic diagram of water molecule alignment along the electrostatic field direction on the sample surface.. Reused with permission from [22].

Surface modulations, such as applying voltage, adsorbates and capping layer over LAO/STO can change the interfacial transport properties. With thickness of 3 unit cells, the band structure of LAO/STO heterostructure should be opened with a small gap

as shown in ref [2]. It is close to the metal-insulator transition and the transition can be driven by applying a voltage [50]. Xie *et al.* [21] discovered that the sheet carrier density increases significantly by different kinds of polar liquid. In 2012, Au *et al.* [22] discovered that the interface conductance becomes non-linear with saturation currents as shown in Figure 1-5 when polar liquids presents at the LAO surface. It was suggested that the interface turns into n-type semiconductor with polar liquid on LAO/STO.

1.2.6 Two-Dimensional Electron Gas (2DEG) at Other Oxide Interfaces

In 2004, 2DEG at the polar/non-polar interface $LaAlO_3/SrTiO_3$ was first reported by Ohtomo and Hwang [1]. After then, thin films of other polar perovskite oxides, such as $KTaO_3$, $LaTiO_3$, $DyScO_3$, on (001) $SrTiO_3$ also show similar transport properties as found in the metallic interface of $LaAlO_3/SrTiO_3$ [51-54]. Some first principles studies also suggested the similarity among these systems [51, 55]. It is surprising that $KTaO_3/SrTiO_3$ interface is metallic with negative charge carriers, although $KTaO_3$ is an I-V perovskite oxide which should lead to the polarity in opposite to LAO or other III-III perovskite oxides [51, 52]. 2DEG might also appears in the interface of III-III / I-V perovskite oxides such as $LaTiO_3/KTaO_3$ and $LaTaO_3/KTaO_3$ suggested by theoretical study [56].

However, the properties of the polar/non-polar interface could be different if $SrTiO_3$ is replaced by $BaTiO_3$ [57]. $LaAlO_3/BaTiO_3$ interface only behaves metallic with low oxygen partial pressure. First-principles study indicated ferroelectric dead

layer formed at $BaTiO_3$ next to the interface [58]. From Figure 1-6, the ferroelectricity of $BaTiO_3$ may interrupt the metal-insulator transition since the sheet resistant reduce at the temperature over the ferroelectric transition temperature [57].

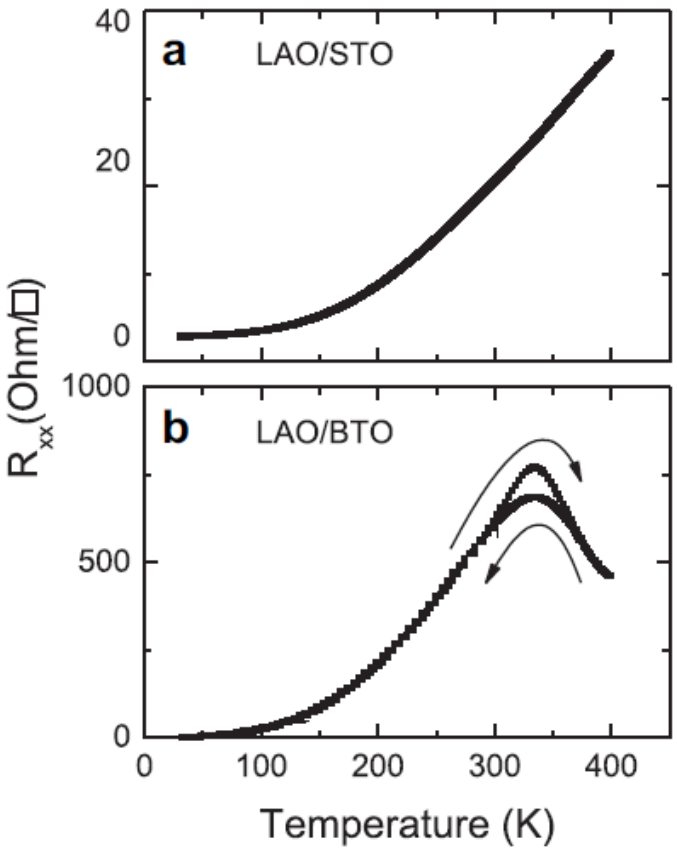

Figure 1-7 The temperature dependence of (a) LAO on STO substrate and (b) LAO/BTO heterostructure on STO substrate up to 400 K. Reprinted from [57], Copyright (2011), with permission from Elsevier.

In 2011, bare STO surface is suggested to have 2DEG [59-63]. Metallic state on the surface of STO can be observed by using angle-resolved photoemission spectroscopy (ARPES) [60, 63], but no electrical transport properties have been

reported to the best of my knowledge. A few theoretical studies indicate that the metallic states may be related to the oxygen vacancies on surface [59, 64].

Most recently, experiments were reported to obtain 2DEG at (110) and (111) LAO/STO interfaces [25] and amorphous LAO on (001) STO surface [24, 65]. The insulator-to-metal transitions at the (110) and (111) LAO/STO interfaces occur with critical LAO thickness of 7 and 9 monolayers, respectively [25]. In (110) LAO/STO interface and amorphous-LAO/STO interface, polar discontinuity should not exist and the conduction of these two systems cannot be explained by polar-catastrophe model. The mechanism of the conduction at these interfaces remains unclear.

1.3 Motivation of the Project

2DEG at LAO/STO heterostructure and other related systems have drawn the attention of researchers since the first report in 2004 [1]. Many variants of (001) LAO/STO heterostructure have been proposed, such as capping layers on LAO/STO [18, 19], LAO on (001) STO with miscut angle [66-68] and adsorption on LAO/STO [21-23].

A deeper understanding of these systems could raise great potential in applications. For example, the change on transport properties due to polar molecules on LAO/STO provides a possibility to fabricate polar molecule sensors [22]. However the physics remains unclear in some variants of the LAO/STO and a lot of questions need to be tackled.

Is there any difference of the mechanisms among different orientations of LAO/STO heterostructures? This question has not been solved yet. Only a few reports on (110) and (111) surface of perovskites have been reported and no theoretical studies on (110) and (111) oriented LAO/STO interfaces have been published. Theoretical study is needed to fill these empty areas.

How do the adsorptions affect the interfacial transport properties of LAO/STO heterostructure? This question has been answered partially. Metallic adatoms [69, 70] and hydrogen atoms [23] on (001) LAO/STO have been studied theoretically, but the mechanism of the dramatic change [21, 22] (see part 1.3.3 of this thesis) on the transport properties due to the polar molecules on the surface of LAO/STO is unknown. First principles studies may help answering this question.

1.4 Outline of the Thesis

Chapter 1 (this chapter) is the introduction of this thesis, including a brief literature review of 2DEG and LAO/STO heterostructure, the mechanism of 2DEG at LAO/STO and the transport properties of LAO/STO and similar systems. Motivation of this thesis is also given.

Chapter 2 is a brief introduction of the theory behind the calculation which is used in this study. It includes the computer software, the theory (Density Functional Theory) and other techniques.

In Chapter 3, the effects of H_2O molecules on LAO/STO heterostructure are studied. Different amount of molecules is considered. The properties of the system are determined.

In Chapter 4, (110) LAO/STO interface is studied. The atomic-smooth (110) interface is considered. Electronic properties are calculated. The mechanism of conduction and electronic properties of (110) oriented LAO/STO interface are also investigated.

In Chapter 5, similar to Chapter 4, (111) LAO/STO interface is studied. Electronic properties and the mechanism of conduction and electronic properties are investigated for (111) LAO/STO interface.

Finally, conclusion and suggestions to future work are given in Chapter 6.

CHAPTER 2 METHODOLOGY

$LaAlO_3/SrTiO_3$ heterostructure and related systems have been investigated by first principles calculation in this thesis. First principles calculations have been done within the framework of Density Functional Theory (DFT) achieved by Vienna ab initio Simulation Package (VASP) [71, 72].

2.1 First Principles Calculations in Materials

First principles or ab initio method means investigation without using empirical assumption or parameters[73]. In order to calculate the properties of solids or clusters by first principles, the systems are treated as electrons and nuclei and their behaviors can be described by quantum mechanics, such as the many-body non-relativistic Schrödinger equation with the Hamiltonian H below.

$$H = -\sum_I \frac{\hbar}{2M_I}\nabla_I^2 - \frac{\hbar}{2m_e}\sum_i \nabla_i^2 - \frac{1}{4\pi\varepsilon_0}\sum_{i,I}\frac{Z_I e^2}{|\vec{r}_i - \vec{R}_I|} + \frac{1}{2}\frac{1}{4\pi\varepsilon_0}\sum_{i\neq j}\frac{e^2}{|\vec{r}_i - \vec{r}_j|} + \frac{1}{2}\frac{1}{4\pi\varepsilon_0}\sum_{I\neq J}\frac{Z_I Z_J e^2}{|\vec{R}_I - \vec{R}_J|} \quad (1)$$

where $\hbar$ is the Plank constant; ε_0 is the vacuum permittivity; M_I are the mass of nuclei;

m_e is the mass of electrons; Z_I are the atomic numbers; $\vec{R}_I$ and $\vec{r}_i$ are the position of nuclei and electrons correspondingly.

The first and second terms are the kinetic terms for nuclei and electrons; the third, fourth and fifth terms are the Coulomb potentials for interaction of electron-nucleus, electron-electron and nucleus-nucleus correspondently.

However, quantum behavior of nuclei is insignificant in most cases, since nuclear mass M_I is much larger than electron mass m_e [74]. In most first principles method, such as Hatree-Fock theory or Density Functional theory, nuclei are treated classically and electrons are described by quantum mechanics.

2.2 Born-Oppenheimer Approximation

It is more convenient to ignore the motion of nuclei (the first term in previous equation), as nuclear mass M_I is much larger than electron mass m_e. This results in the approximation called Born-Oppenheimer or adiabatic approximation[74, 75]. With this approximation, the Hamiltonian becomes:

$$H = -\frac{\hbar}{2m_e}\sum_i \nabla_i^2 - \frac{1}{4\pi\varepsilon_0}\sum_{i,I}\frac{Z_I e^2}{|\vec{r}_i - \vec{R}_I|} + \frac{1}{2}\frac{1}{4\pi\varepsilon_0}\sum_{i\neq j}\frac{e^2}{|\vec{r}_i - \vec{r}_j|} + \frac{1}{2}\frac{1}{4\pi\varepsilon_0}\sum_{I\neq J}\frac{Z_I Z_J e^2}{|\vec{R}_I - \vec{R}_J|}$$

$$= T + V_{ext} + V_{int} + E_I \qquad (2)$$

or $H = H_e + E_I$

where T, V_{ext}, V_{int}, E_I are the second to fifth terms in Eq. (1) or the first to fourth terms in Eq. (2); H_e includes the first three terms related to interaction on electrons, and E_I is simply reduced to the classical Coulomb potential of nuclei.

States of electrons are possibly to be determined by H_e with the nuclei at certain positions R_I. If the wave functions Ψ of electrons are obtained, the energy of the system can be determined as

$$E = < \Psi | H_e | \Psi > + E_I \quad (3)$$

Many useful quantities can be derived from the system energy. For example, the force (by electrons) on a nucleus at R_I can be obtained via Hellmann-Feynman theorem, and the force on the nucleus at R_I due to other nuclei can be calculated classically[74]. Therefore, the force on the nucleus at R_I is

$$F = - < \Psi \left| \frac{\partial H_e}{\partial R_I} \right| \Psi > - \frac{\partial E_I}{\partial R_I} \quad (4)$$

The force obtained can be used for optimization of the systems or dynamics calculations such as ab initio molecular dynamics (ab initio MD).

2.3 Density Functional Theory

The problem of first principles calculation for solids or clusters is reduced to a Schrödinger equation of many electrons, as shown below.

$$H_e = -\frac{\hbar}{2m_e}\sum_i \nabla_i^2 - \frac{1}{4\pi\varepsilon_0}\sum_{i,I}\frac{Z_I e^2}{|\vec{r}_i - \vec{R}_I|} + \frac{1}{2}\frac{1}{4\pi\varepsilon_0}\sum_{i\neq j}\frac{e^2}{|\vec{r}_i - \vec{r}_j|} = T + V_{ext} + V_{int} \quad (5)$$

T is the kinetic term, and V_{ext} is the Coulomb potential due to nuclei which is independent to electrons at this stage. The interaction between electrons V_{int} is the most problematic term since it depends on the state of electrons, but the state of electrons is to be determined by H_e.

One may apply the independent electron approximation to split the N-electron Schrödinger equation to N one-electron Schrödinger equations and to solve the N equations one by one from the one with lowest Eigen energy, but it gives no correlation (the third term in (5)) between electrons[74]. Since electrons are indistinguishable, and electrons are Fermions which follow Pauli exclusive principle. It requires the wave function $\Psi(\vec{r}_1, \vec{r}_2, \cdots \vec{r}_N) = 0$, for $\vec{r}_i = \vec{r}_j$ and i≠j, and $|\Psi(\vec{r}_1, \vec{r}_2, \cdots \vec{r}_N)|$ remains unchanged with exchanging any two coordinates $\vec{r}_i$, $\vec{r}_j$. N-electron wave function may therefore be expressed as the determinant (known as Slater determinant) of the N one-electron wave functions in N coordinates as shown below [74, 75].

$$\Psi(\vec{r}_1, \vec{r}_2, \cdots \vec{r}_N) = \frac{1}{\sqrt{N!}} \begin{vmatrix} \psi_1(\vec{r}_1) & \cdots & \psi_1(\vec{r}_N) \\ \vdots & \ddots & \vdots \\ \psi_N(\vec{r}_1) & \cdots & \psi_N(\vec{r}_N) \end{vmatrix} \quad (6)$$

It is Hartree-Fock approximation, if the V_{int} is approximated by self-consisting mean field potential (guess the wave function and electron density to calculate the potential due to average guess electron density, and use the solution or combine it with old guess as new guess). The (average) electron density n is

$$n(r) = \sum_i |\psi_i(\vec{r})|^2 \quad (7)$$

The Hamiltonian H_{HF} under Hartree-Fock approximation is

$$H_{HF} = -\frac{\hbar}{2m_e}\sum_i \nabla_i^2 - \frac{1}{4\pi\varepsilon_0}\sum_{i,I}\frac{Z_I e^2}{|\vec{r}_i - \vec{R}_I|} + \frac{1}{2}\frac{1}{4\pi\varepsilon_0}\int \frac{n(\vec{r}_i)n(\vec{r}_j)e^2}{|\vec{r}_i - \vec{r}_j|} d\vec{r}_i d\vec{r}_j \quad (8)$$

In Density Functional theory (DFT), however, the correlation of electrons is included, at least in principle, and the convenience of independent electron approximation is kept. By the two Hohenburg-Kohn Theorems, the ground state electron density $n_0(r)$ determines the V_{ext} (and therefore the H_e), and there is a universal energy functional E[n] for any V_{ext}, that $E[n_0]$ is the global minimum and equals to the ground state energy of H_e. If the form of the energy functional is known, the ground state density n_0 and the ground state energy E_0 can be obtained by minimizing E[n]. This is the main spirit of DFT. Once the n_0 and E_0 are obtained, many properties can be derived from them, and the aims of first principles calculations can be achieved.

However, the form of the energy functional is not known, so approximation is applied in DFT calculations. The energy (only consider the many-electron system) in functional form is

$$E[n_0] = T[n_0] + V_{ext}[n_0] + V_{int}[n_0] \tag{9}$$

Consider the Kohn-Sham approach, which assumes that there is a many-body system without interaction equivalent to the original many-body interacting system which gives the same energy E and the same electron density n. The original potential (V_{ext}+V_{int}) is only replaced by an effective potential (V_{KS}) in formula, but the "electrons" in the new system act independently. The formula of Kohn-Sham Hamiltonian H_{KS} is H_{HF} added by the exchange and correlation term E_{XC}.

$$H_{KS} = -\frac{\hbar}{2m_e}\sum_i \nabla_i^2 - \frac{1}{4\pi\varepsilon_0}\sum_{i,I}\frac{Z_I e^2}{\left|\vec{r}_i - \vec{R}_I\right|} + \frac{1}{2}\frac{1}{4\pi\varepsilon_0}\int\frac{n(\vec{r}_i)n(\vec{r}_j)e^2}{\left|\vec{r}_i - \vec{r}_j\right|}d\vec{r}_i d\vec{r}_j + E_{XC} \tag{10}$$

and the ground state energy is:

$$E[n_0] = T[n_0] - \frac{1}{2}\frac{1}{4\pi\varepsilon_0}\sum_I\int\frac{n_0(\vec{r}_i)Z_I e^2}{\left|\vec{r}_i - \vec{R}_I\right|}d\vec{r}_i + \frac{1}{2}\frac{1}{4\pi\varepsilon_0}\int\frac{n_0(\vec{r}_i)n_0(\vec{r}_j)e^2}{\left|\vec{r}_i - \vec{r}_j\right|}d\vec{r}_i d\vec{r}_j + E_{XC}[n_0] \tag{11}$$

Since it is non interacting system in Kohn-Sham approach, the N-electron wave function is a determinant of N by N single electron wave functions as Eq. (6), but it is not the independent electron approximation in DFT. The electron density n can also be expressed by N one-electron wave functions ψ_i as Eq. (7). By applying variational principle to the energy functional in Eq. (11), the N-electron Schrödinger equation can be separated into N one-electron Schrödinger-like equations (Kohn Sham equation) as show in Eq. (12) below [75, 76].

$$\left(-\frac{\hbar}{2m_e}\nabla^2 - \frac{1}{4\pi\varepsilon_0}\sum_I \frac{Z_I e^2}{|\vec{r}-\vec{R}_I|} + \frac{1}{2}\frac{1}{4\pi\varepsilon_0}\int \frac{n(\vec{r}_j)e^2}{|\vec{r}-\vec{r}_j|}d\vec{r}_j + \frac{\delta E_{XC}[n]}{\delta n}\right)\psi_i(r) = \varepsilon_i\psi_i(\vec{r}) \quad (12)$$

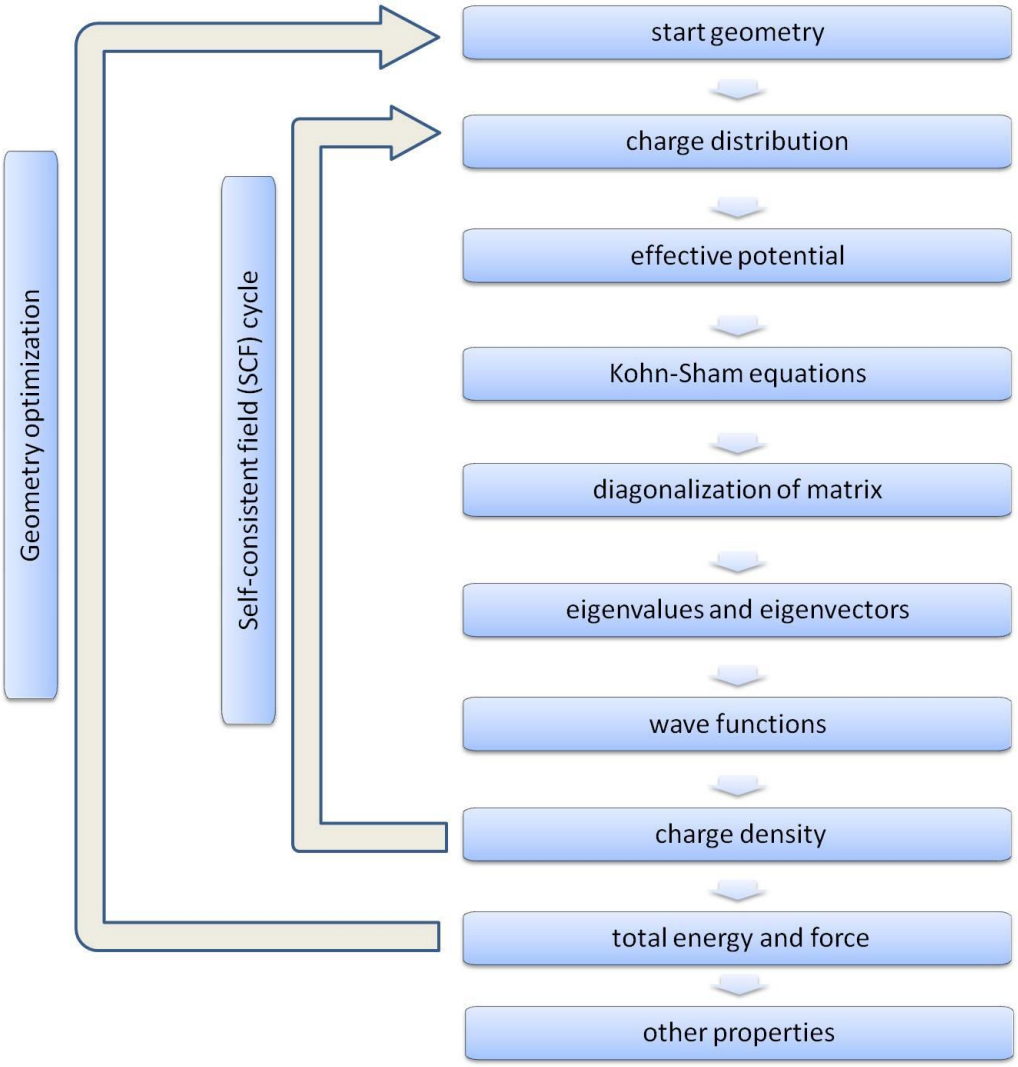

Figure 2-1 Scheme of typical electronic calculations. The outer cycle represents the geometry optimization or other manipulation of geometry. The inner cycle is the self-consistency procedure to solve the Kohn-Sham equation. [74, 77].

The exchange and correlation term E_{XC} in Eq. (12) is not known in general, but it can be approximated by different approaches such as Local Density approximation (LDA) or Generalized Gradient approximation (GGA)[75]. DFT can be extended to spin-polarized systems, with consideration of both electron density and spin density. By self-consistent process, as shown in Figure 2-1, the energy functional E[n] is minimized

with the set of one-electron wave function ψ_i obtained from (12) to solve the many-electron system. The total ground state energy of N electrons (non spin-polarized) is

$$E = 2\sum_{i=1}^{N/2}\varepsilon_i - \frac{1}{2}\frac{1}{4\pi\varepsilon_0}\int\frac{n(\vec{r}_i)n(\vec{r}_j)e^2}{|\vec{r}_i-\vec{r}_j|}d\vec{r}_i d\vec{r}_j + E_{XC}[n] - \int\frac{\delta E_{XC}[n]}{\delta n}n(\vec{r})d\vec{r} \qquad (13)$$

2.4 Basis, Pseudopotential and Projector Augmented Wave Method

The wave functions of electrons are not analytical functions, except very few simple systems, such as a hydrogen atom. During computation, wave functions can be denoted directly as digits for each grid point in the space (or in reciprocal space) being considered or decomposed in different sets of basis, like plane wave basis, atomic orbital basis (LCAO) or Gaussian basis. Plane wave basis is implemented in VASP, the code for all first principles calculations in this project. More issues about plane wave basis are shown in the following in this session.

In a crystal, the (one electron) wave function ψ_k, by Bloch Theorem, is

$$\psi_k(\vec{r}) = u_k(\vec{r})e^{i(\vec{k})\cdot\vec{r}} \qquad (14)$$

where $u_k(\vec{r})$ is periodic with period equals to the lattice vector $\vec{R}$. Expressing u_k in Fourier series, it becomes Eq. (15) below.

$$\psi_k(\vec{r}) = \sum_m c_m e^{i(\vec{k}+\vec{G}_m)\cdot\vec{r}} \quad (15)$$

where $\vec{G}_m$ is the reciprocal lattice vector.

It automatically spans in plane wave basis. In computation, it includes only finite terms with $|\vec{k} + \vec{G}_m| < q$, and q is the cutoff wave number. Cutoff energy E_{cutoff} is defined as $\frac{\hbar^2}{2m_e}q^2$ which is more commonly shown in DFT calculations with plane wave basis [10, 38, 39, 45].

The use of plane wave basis set has some advantages, compared to other basis sets like those localized basis sets, for example, atomic orbital or Gaussian-type basis. It is a complete orthonormal basis set to span any periodic functions. The accuracy can be simply controlled by cutoff energy E_{cutoff} or cutoff wave number q, as it converges as $q \to \infty$, and it is easy to formulate. For example, performing Fourier transforms between real space and reciprocal space or calculating matrix elements of different observables[73, 78]. It is easy to calculate 3-dimensional periodic systems (bulk crystalline solids). However, it also induces some drawbacks or disadvantages. The boundary condition of simulation box is restricted to 3-dimensional periodic. To simulate systems of lower dimension, such as surfaces (H_2O on LAO/STO surface in Chapter 3 of this report), huge box of simulation with vacuum is required to reduce the interaction between different periods that results in significant increase of computational demand. Huge simulation box can also increase the basis size for the same cutoff, since the difference between $\vec{G}_m$ in Eq. (15) decreases with size. Most electrons behave localized around nuclei, but plane waves are extending in space, so it

requires a large set of plane waves (high cutoff energy) to span the wave functions.

The core electrons of atoms are of less interesting for most purposes of studies, since they hardly change in different situations, such as in chemical reactions. It should improve the speed of calculation, if only valence electrons are considered, with core electrons ignored. In early days, the method known as orthogonalized plane waves (OPW) was used, which simply orthogonalize the plane waves basis to the core wave function [73, 74].

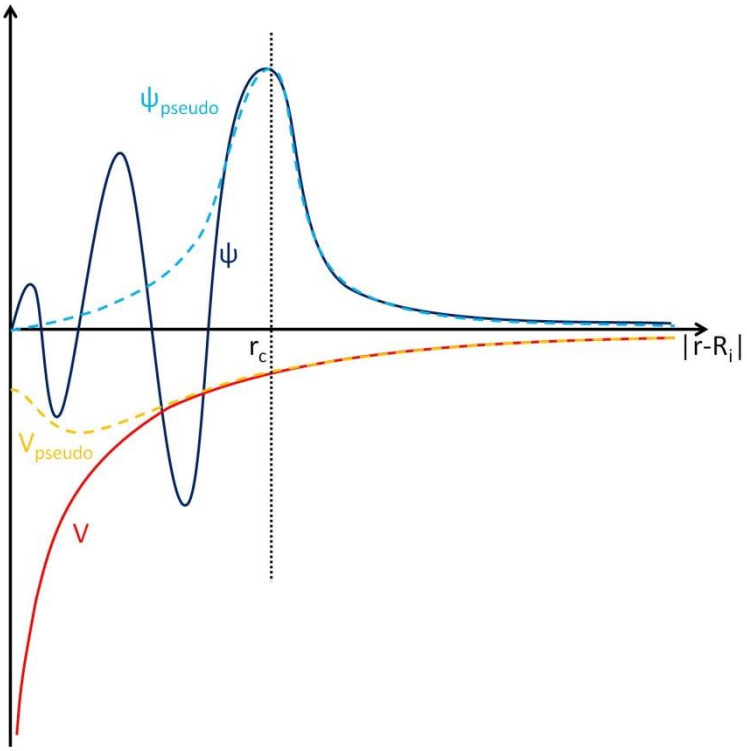

Figure 2-2 The pseudowavefunction (blue dash line) and the true wavefunction (blue solid line), and the corresponding pseudopotential (orange dash line) and true potential (red solid line) from an atom at R_i. The cutoff radius is r_c.

Pseudopotential method is developed to increase the efficiency of computation by reducing the number of electrons and the size of basis, therefore especially important

for plane wave basis. In pseudopotential approximation, the Kohn-Sham effective potential (last three terms in left side of Eq. (12)) is further replaced by an effective potential (called pseudopotential) that keeps wave functions of valence electron outside a certain cutoff radius r_c from a nucleus, like Figure 2-2, but the core electrons and the singularity of Coulomb potential are removed from the effective systems. It restricts to keep the norm of wave function within cutoff radius in the approach of norm-conserve pseudopotential. The ultrasoft pseudopotential, faster but less accurate in general, aims to mostly smoothen the wave functions within the cutoff region, leading to reduce the number of plane waves to span wave functions. Correction of relativistic effect can also be included in the pseudopotential[74, 77].

By generalizing the OPW and pseudopotential, projector augmented wave (PAW) method [79, 80] is developed to improve the accuracy, and keep the efficiency. PAW is also employed in VASP code for the calculation of this work.

Blöchl [79] proposed the projector augmented wave method and stated that "The physically relevant wave functions in this Hilbert space exhibit strong oscillations, which make a numerical treatment cumbersome. Therefore, we transform the wave functions of this Hilbert space into a new, so-called pseudo (PS) Hilbert space." This is the basic idea of PAW method. A linear transformation $\mathcal{T}$ is used to transform pseudo wave functions ($\tilde{\psi}$) to wave functions in all-electron method (ψ).

The transformation $\mathcal{T}$ is chosen to be some local atom-center contribution $\hat{\mathcal{T}}_R$ within augmentation region Ω_R but unchanged elsewhere, so,

$$\mathcal{T} = \mathrm{I} + \sum_{\mathrm{R}} \hat{\mathcal{T}}_{\mathrm{R}} \tag{16}$$

Similar to pseudopotential and OPW, $\hat{\mathcal{T}}_{\mathrm{R}}$ are chosen that transform some $(\tilde{\psi}_{\mathrm{n}})$, which are smoothen in Ω_{R}, to some (ψ_{n}), which usually are the valence atomic orbitals of an isolated atom orthogonal to core states. Core electrons are treated in a similar way, but the wave functions of core electrons are not changed in the self-consistent process in calculation[80]. Most calculations are done with psedo wave functions and pseudo operators in pseudo Hilbert space, so the efficiency is close to ultrasoft pseudopotential methods. The results can be projected back to Hilbert space of all-electron method, so the results are consistent to all-electron calculations with frozen core approximation.

2.5 Other Techniques

For periodic systems, summation of the Eigen values ε_{i} in (13) is replaced by integration of $\varepsilon_{\mathrm{k,i}}$ for the k over the Brillouin zone for all occupied band, and in formalism, should be done by calculating the total energy per period (unit cell). In computation, Eigen values can be obtained at a finite number of k-points, and interpolation may be done between discrete k-points. However, some problems rise then. For example, the choice of k-points may affect the efficiency and accuracy of calculation. If there are partial occupied bands, such as those in metals, the integration has to stop till Fermi-level. It may also cause numerical instability and difficulty in converging, since the occupation of the states around Fermi-level may change rapidly during iteration to search the ground state.

There are many ways to sample the k-points. Monkhorst and Pack[81] suggested a $q_1 \times q_2 \times q_3$ mesh points (Monkhorst-Pack mesh) given by

$$\vec{k} = u_1\vec{G}_1 + u_2\vec{G}_2 + u_3\vec{G}_3$$

where $\vec{G}_1, \vec{G}_2, \vec{G}_3$ are the reciprocal lattice vectors, and

$$u_i = \frac{2r - q_i - 1}{2q_i}, r = 1,2, \dots q_i, \qquad i = 1,2,3$$

This gives an unbiased sampling in the Brillouin zone, and the mesh is symmetric. Some points would be equivalent, for the lattice with symmetry. The even Monkhorst-Pack mesh point is more efficient than odd Monkhorst-Pack mesh point, in general[73, 74]. For example, both of the meshes of 3×3×1 and 4×4×1 for square lattice can be reduced to only three inequivalent k-points, but 4×4×1 is certainly denser than 3×3×1. It should be noticed that even Monkhorst-Pack meshes do not include gamma point (0,0,0) in Brillouin zone, but it is necessary to include gamma point for some geometry, such as hexagonal lattice. Therefore, the choice of k-points should be concerned, although sometimes it is not mentioned in reports.

To improve the numerical stability, especially in metallic systems, smearing of the states can be applied. Fractional occupations of states occur with smearing, so that density of states is smoothened and the occupations of states around Fermi-level change continuously during iteration. Many schemes of smearing are possible. For example,

Fermi smearing produces the smearing such that occupation of states follows Fermi distribution. Gaussian smearing, applied in this work, smears a state which has the density of state as a Gaussian function. The degree of smearing is related to the parameter called smearing width. Occupation of states above Fermi-level depends on the scheme of smearing, but there should be more occupation above Fermi-level for larger smearing width in general. As Density Functional Theory (DFT) is derived for a system at ground state, occupation above Fermi-level would produce error. For accurate calculation, a dense mesh of k-points and a small width of smearing should be used.

For low dimensional systems, such as surface or molecules, a large box of simulation is required as stated in session 3 of this Chapter. Increasing the box size and with more vacuum in the box can reduce some interactions between periods, such as electrons tunneling through vacuum between two periods. However, some interactions between periods cannot be reduced significantly by increasing the box size and vacuum. Electric dipole (due to asymmetric structure) is an example. In Chapter 3, the LAO/STO thin films with or without H_2O become parallel slabs. Each slab is a layer of dipoles. Interaction between dipoles decays quickly with distance, but interaction between layers of dipoles decays hardly. Dipole correction [82-85] is applied for asymmetric structure by adding a potential corresponding to a field with the same strength in opposite direction to cancel the interaction between dipoles. Figure 2-3 shows (a) the potential without dipole correction, (b) the potential of dipole correction and (c) the potential with dipole correction. As restricted by periodic boundary condition, the potential is sloped around boundary in Figure 2-3 (a), but it become discontinuous near boundary in Figure 2-3 (c), and the potential tends to be flat till the discontinuous point. This shows

that the interaction between periods is interrupted, and the electric field between slabs is cancelled by dipole correction. The properties of a slab, instead of the system of parallel slabs, can be appropriately simulated by adding dipole correction.

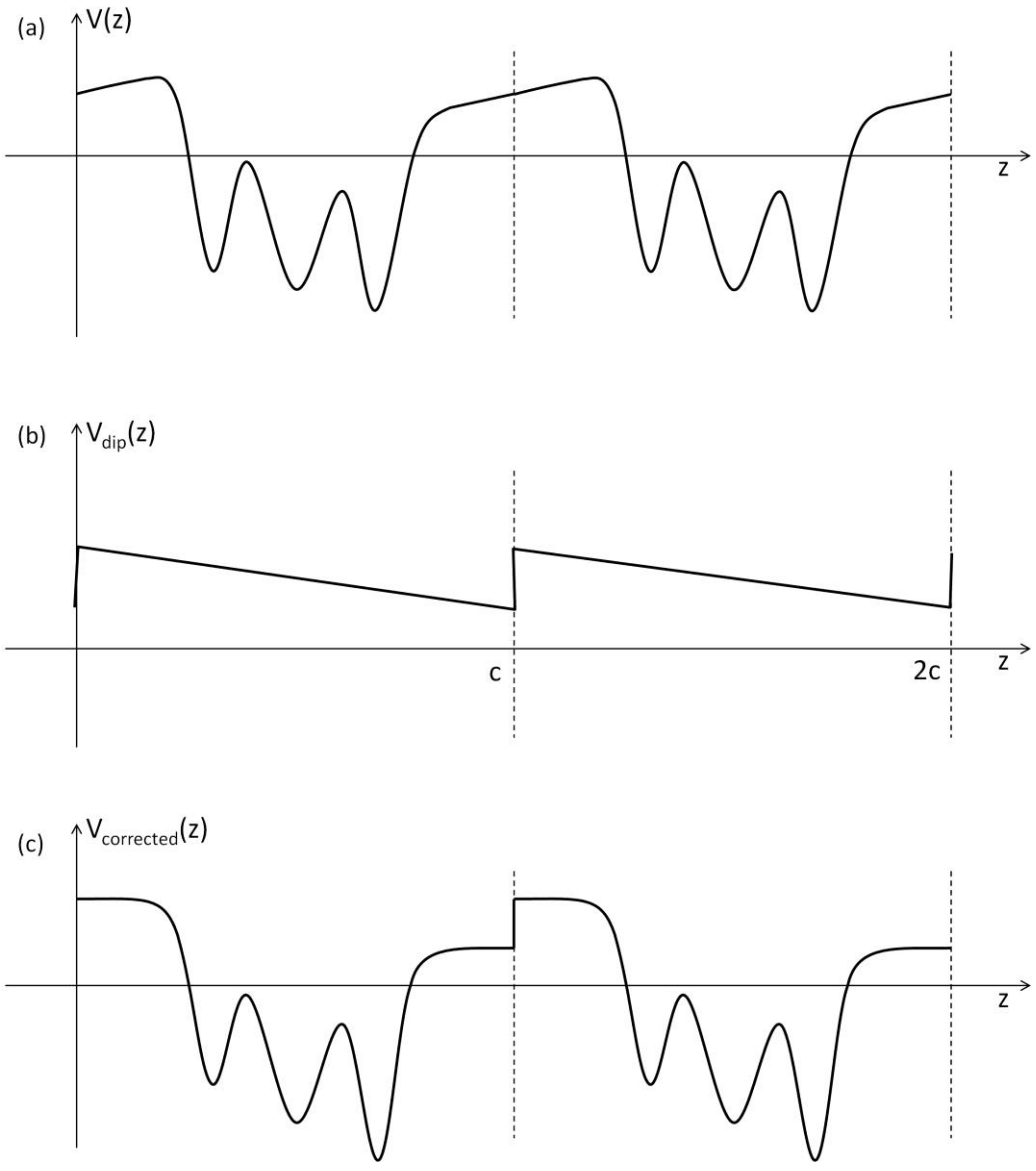

Figure 2-3 Schematic diagram of (a) xy-averaged (parallel to the surface) electrostatic potential, (b) the potential added as dipole correction which separates the work functions of the clean and adsorbate-covered surfaces, and (c) the corrected electrostatic potential [82, 84, 85].

.

CHAPTER 3 TRANSPORT PROPERTIES OF $LaAlO_3/SrTiO_3$ HETEROSTRUCTURE WITH WATER ADSORBATES

3.1 Introduction

Recently, experimental reports show the importance of the correlation between the interface of $LaAlO_3/SrTiO_3$ (LAO/STO) and the surface charge states. Therefore the modification of the conduction at the interface have been attempted through introducing surface charges and adsorbates [2, 16, 20, 86, 87] or a capping layer on LAO/STO such as STO [18]. The fact that the interface conducting states can be changed dramatically with the surface adsorbates leads to a possible application of LAO/STO interfaces as polar molecule sensors and a new generation of electronics [2, 86]. Xie *et al*. [21] reported a three times change of conductivity at the LAO/STO interface induced by the surface adsorption of water. The change of conductivity is believed to be induced by an increase of the sheet carrier density of the 2DEG by more than 2×10^{13} cm^{-2}, suggesting that the adsorbent has a great influence on the charge transfer from the film surface to the interface.

In 2012, Au *et al.* [22] reported an in-plane field effect transistor structure, where the polar molecules act as a gate voltage to affect the source/drain current across the interface channel. A model was also proposed to interpret the dramatic change in the

I-V characteristics, where a Schottky junction is believed to form between the 2DEG and the water adsorbates affected interface. These observations provide a direct evidence of the built-in electric field in the LAO layer and suggest that system of LAO/STO interface can be used for high-performance polar molecule sensors. In this chapter, in order to provide a theoretical explanation to these experimental results, the influence of water molecules on the electronic transport properties of $LaAlO_3/SrTiO_3$ heterostructure have been studied by first-principles calculations.

3.2 Calculation Details

First-principles calculations are performed within the framework of density functional theory and local density approximation (DFT-LDA) using the Vienna *ab initio* Simulation Package (VASP) [71, 72]. The supercell shown in Figure 3-1 contains 4 unit-cells of LAO on 4 unit-cells of STO substrate with the in-plane lattice constants fixed at their theoretical values, a=b=3.8633Å. For the structures with water, water molecule(s) are added on the top of the LAO layer. The thickness of the vacuum region between the slabs is about 20Å. The cut-off energy of the plane wave basis is 500 eV; the k-point mesh is 11×11×1 Monkhorst-Pack mesh; and Gaussian smearing is applied with small smearing width of 0.05eV during calculation of energy. A dipole correction is applied along the out-of-plane axis to cancel the dipole-dipole interaction due to the dipole moment in each slab. [82, 83]

The first consideration to build the model of H_2O on LAO is to allow the H_2O be fully optimized by lowest energy criterion without restriction of the symmetry. Many different models have been tried, and eventually models a and b come out to have the lowest energy among all calculated models with one and two H_2O per (1×1) surface unit, respectively. Dissociative adsorption [88, 89] was considered but found energetically unfavorable, and it should also be pointed out that the H_2O molecules were not decomposed on the surface of LAO, and the dissociation of hydrogen [23] did not occur during optimization. Having determined the first layer of water molecules bonding on the LAO with lowest energy, we put the second layer of H_2O by forming hydrogen bond. Due to the relative weak hydrogen bond and easy rotation of the bonding angle (the characteristics of liquid water), it is assumed that the bonding angle will be more determined by aligning the polarization direction to the electric field direction of the LAO layer that leads to a picture suggested by Xie *et al* [21].

3.3 Results and Discussion

Figure 3-1 shows optimized atomic structure of four models, where model a contains one H_2O molecule; model b contains two H_2O molecules on the (1×1) LAO surface and model c contains two layers of H_2O molecules. In the optimized structures, O_x (notation of O_x and O_y representing two O atoms on AlO_2 terminated surface shown in Figure 3-1) in models a and b shift upward due to the attraction from H of H_2O. It should be noted that the structure of model a is consistent with that from other theoretical studies of H_2O

molecular adsorption on surface of other perovskites [88, 89]. The initial structure of model b is similar to that of a monolayer of H_2O adsorbed on $SrTiO_3$ from ref [89], where one H_2O is attached to a B-site (Ti) atom and forms hydrogen bond with another H_2O which also forms hydrogen bond with an O ion on the LAO surface.

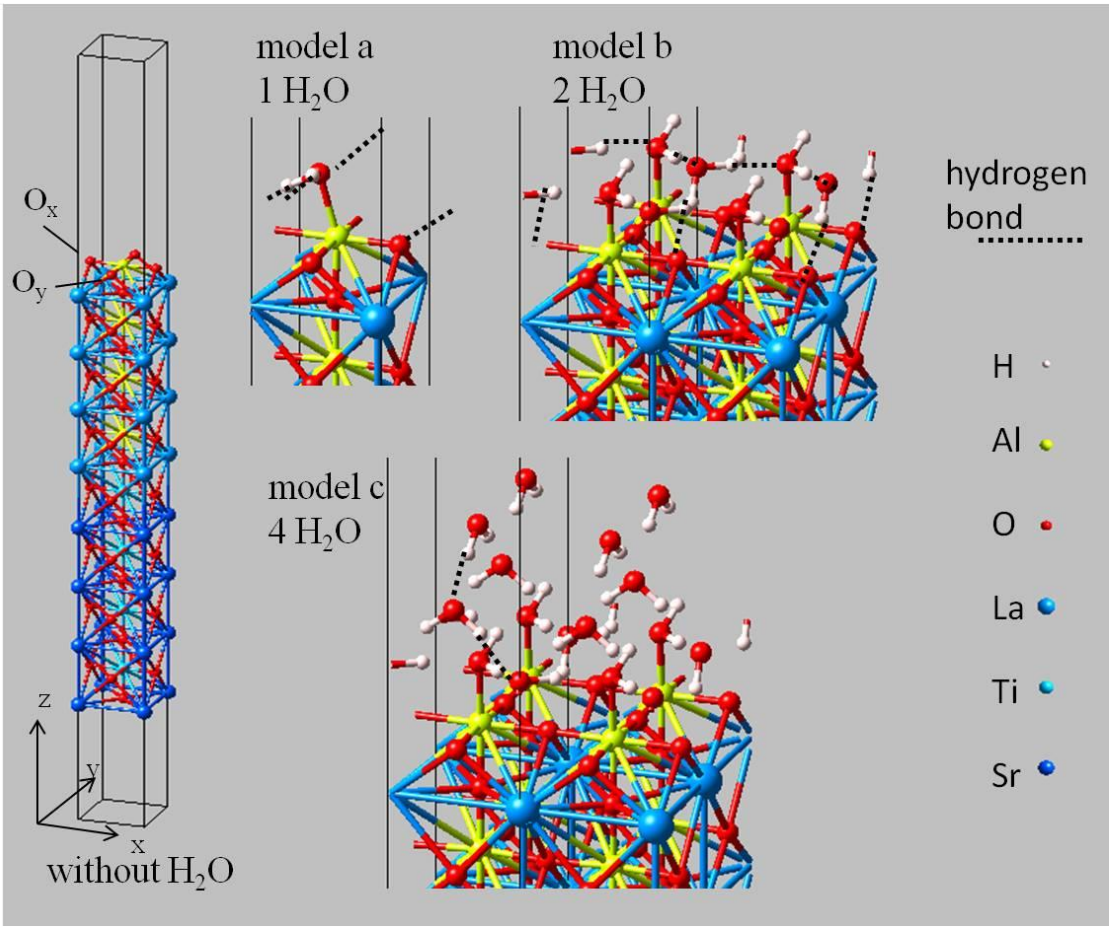

Figure 3-1 Atomic structure of four models. Model a contains one molecule on (1×1) LAO surface, models b contains two molecules on (1×1) LAO surface and model c contains four molecules. Neighbouring periods for model b and c are shown for convenience. Dash lines represents hydrogen bonds, and dash circles represents atoms shift outside the region for display. O_x and O_y represent two Oxygen atoms on surface which form bonds with Al in x and y directions.

The binding energy ($E_{binding}$) per H_2O on the LAO/STO heterostructure is $E_{binding} = (E_{without\ H2O} + n\ E_{isolated\ H2O} - E_{with\ H2O})/n$ and n is the number of H_2O per (1×1) unit cell. The binding energy in model a is 1.43eV; while it is 1.40 eV in model b with two H_2O resulted from both the adsorption of the H_2O on the surface and the hydrogen bonds between the H_2O molecules. Since the H_2O bonded with Al atom is similar to that in model a, and another H_2O is linked by hydrogen bond, the slightly decrease of the binding energy indicates that the adsorption energy of H_2O should be in the same order of the hydrogen bond energy. It is also well known that LDA overestimates the binding energy in general [90, 91], therefore the actual binding energy of the adsorbed water molecule on the LAO surface should be weaker, and it is expected that the water molecule can be easily desorbed by thermal energy. This explains the experimental fact that by heating the sample to over 100°C, the water molecule induced I-V characteristics [22] disappears and a normal metallic conduction of the interface resumes.

It should be noted that models a and b have the lowest energy for one and two molecules per (1×1) unit cell. Model a is the most possible model for one monolayer of water; while model b is the most possible model for two layers of water. More layers of water molecules need very large number of atoms in the model and large amount of calculations which are beyond our computing limit. Instead, we argue that the aligning of the water molecule along the polarization of the LAO film through hydrogen bonding with the oxygen of LAO could happen, we also include model c where four layers of water molecules align in the same direction forming a hydrogen bonding with LAO.

Even not in a lowest energy state, this model can illustrate the importance of polarization alignment of water molecules.

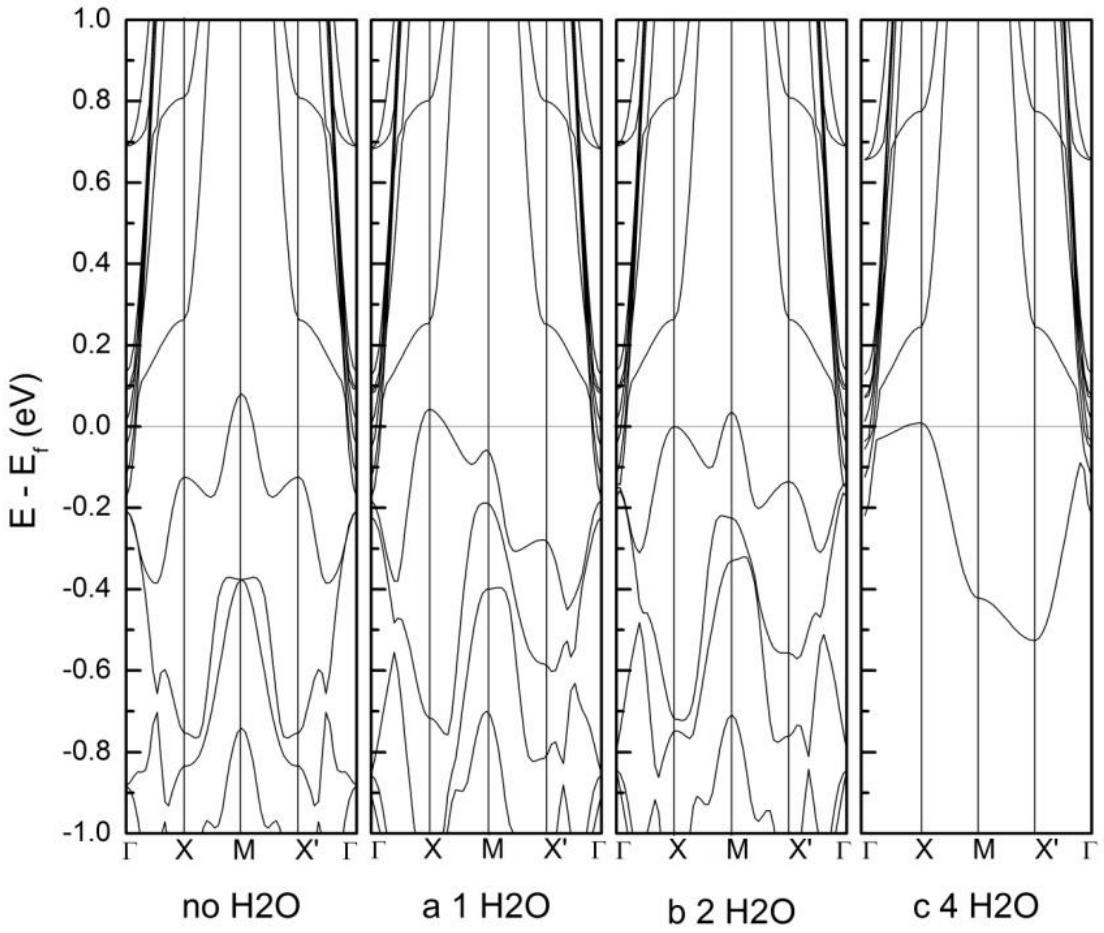

Figure 3-2 Band structures of different models, from left to right : model without H_2O molecules, model a (1 H_2O) , model b ($2H_2O$) and model c ($4H_2O$).

Figure 3-2 shows the band structure before and after adding H_2O (models a-c). The band structure without water is in agreement with other calculations [47, 92] in that the Ti energy bands (conduction band) at the surface layer cross the Fermi-level (E_f)

around the Γ-point (0,0), and the O 2p band (valence band) crosses E_f at M. These results indicate that the presence of conducting electrons in STO at the LAO/STO interface and holes are left at the surface of LAO. The hole states however have not been reported to contribute to the electrical transport on surface of LAO/STO. The holes may be localized as a result of surface impurities, surface roughness or corrected band theory [92]. It can be seen that there is no significant change to the conduction band structure after adding H_2O. However, the hole states, in the valence band at M (0.5,0.5) shift downward in models a and b. The valence band of model a and b rises at X (0,0.5) as shown in Figure 3-2, and this change may depend on the orientation of H_2O molecule on the top surface where the H atoms of H_2O are closer to the O atoms of the AlO_2 surface. Surface states can be affected by even one additional H_2O molecule per (1×1) surface unit. Valence bands in model c of Figure 3-2 do not correspond to any bands in the film without water because those bands in model c are contributed by states in H_2O.

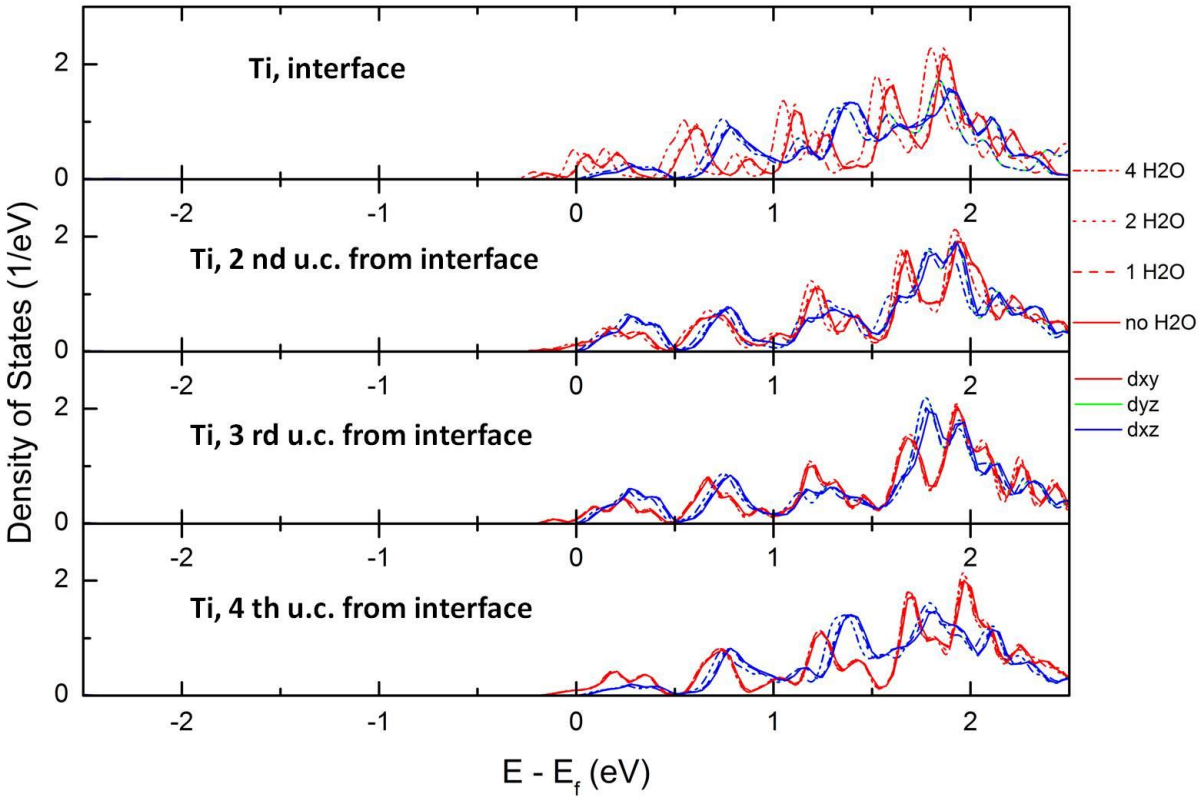

Figure 3-3 Projected density of states (PDOS) of Ti without or with water molecules on LAO surface (models a - c). PDOS of Ti d_{yz} and d_{xz} are overlapped.

Figure 3-3 shows the projected density of states (PDOS) of Ti with and without water molecules adsorbed on the LAO surface. Similar to Ref. [18, 47, 92], the result shows that the conduction electrons occupy most at Ti d_{xy} orbitals since d_{xy} is in lower energy. No observable change from the PDOS of Ti can be found after adding water in models a and b in Figure 3-3. It is also illustrated that Ti d_{yz} and d_{xz} states are overlapped. The dipole field from H_2O should be screened by the dielectric LAO and it could not affect the interface directly. In Figure 3-3, the Ti d_{xy} state in model c shifts down in energy at the interface; and it shows that the additional conduction electrons mostly occupy the Ti d_{xy} states at interface.

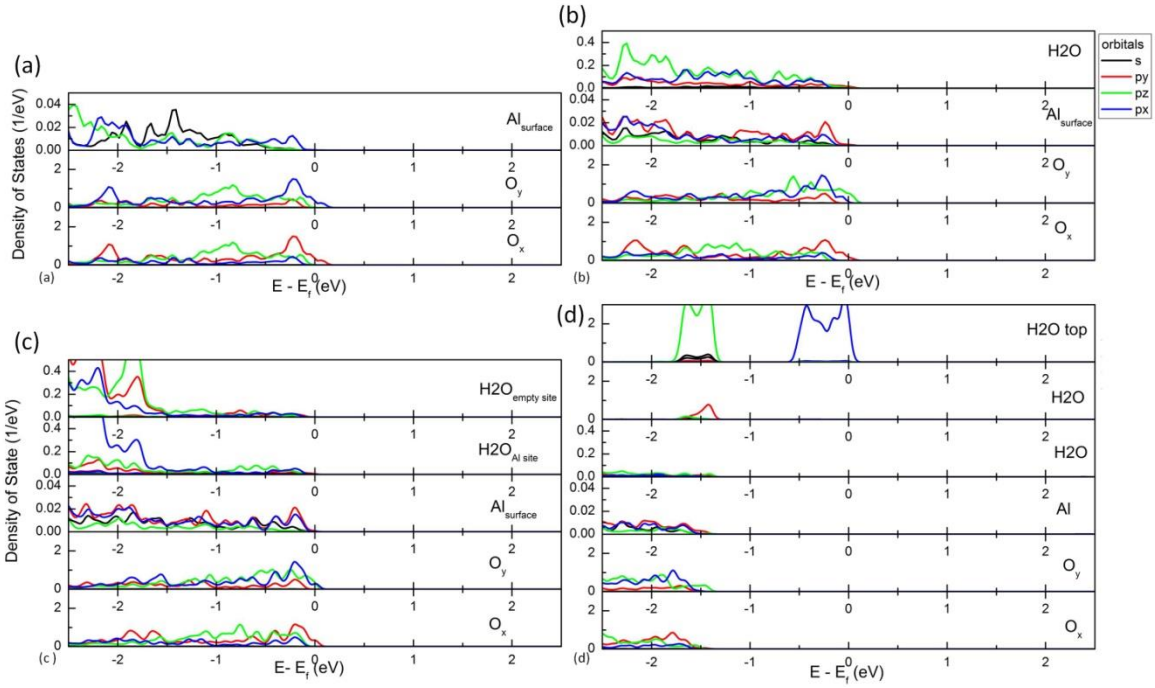

Figure 3-4 Projected density of states (PDOS) of H_2O and AlO_2-terminated surface of models a (b), b (c) and c (d); and (a) the PDOS of AlO_2-terminated surface without H_2O.

Figure 3-4 shows the PDOS of the water molecule and the AlO_2 group at the surface in models a - c, while the results of models b is similar to that of model a. As shown in Figure 3-4 (b), the peaks corresponding to the p_y (p_x) orbitals of the O_x (O_y) atom are right at the Fermi level, indicating the presence of holes on the surface without H_2O. It is interesting to see that the p_z orbital of O_y (O_x) in models a and b shift upward in energy and beyond the Fermi-level. This should reflect the change of the surface hole states of models a - b in the band diagram in Figure 3-2. However, all O 2p states in model c are below the Fermi level in Figure 3-4 (d), but a higher peak of the DOS around the Fermi level appears in the upper H_2O. This indicates that polarity discontinuity at LAO/STO interface is compensated by electrons transferred from H_2O,

instead of the surface of LAO.

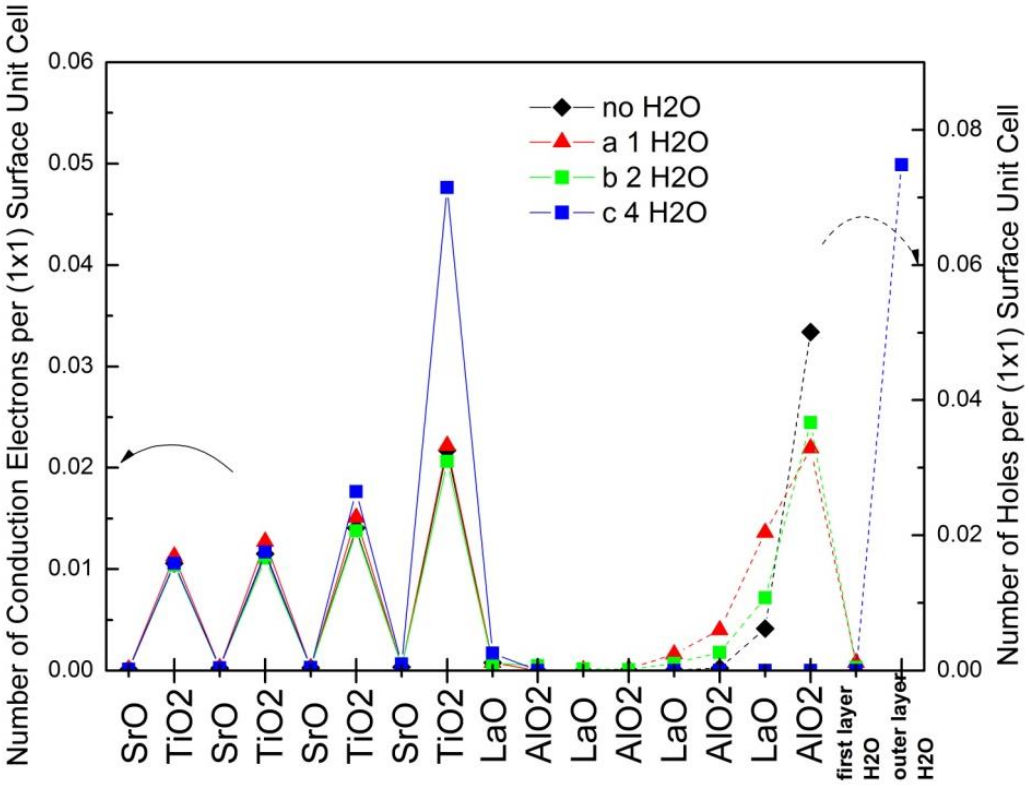

Figure 3-5 Distribution of conduction electrons with solid lines and holes with dashed lines.

Figure 3-5 is an estimation of the amounts of conduction electrons and holes determined by an integration of their corresponding PDOS around the Fermi level showing the result in consistence with literature [93, 94]that most conduction electrons are located at the interface; while away from the interface, conduction electrons decrease in amount. It is apparent that the density of conduction electrons n_{2d} is approximately equal to the density of holes n_h with difference (error) less than 12.5% in each models. n_{2d} and n_h change less than the error in models a and b. Significant change happens in model c, where n_{2d} and n_h increase significantly by 52% and 32%,

respectively. This result qualitatively matches the experimental work [21] where the density of conduction electrons n_{2d} increases from 1×10^{13} cm^{-2} to 2.5×10^{13} cm^{-2}.

Table 3-1 Dipole moment and work function of different models

Model	a	b	c
Change of Dipole Moment along -z(eÅ)	-0.05	-0.08	0.23
Net H_2O Dipole Moment(eÅ)	0.05	0.05	0.59
Change of Work Function (eV)	-0.55	-0.95	2.88

The results illustrated in Figure 3-5 can be intuitively interpreted by two points. First, the additional conduction electrons at the interface with H_2O should come mainly from the states (mostly O 2p orbitals) at the few topmost LAO atomic layers, since those states are sensitive to surface environment such as the different orientations of H_2O. Details of the dipole moment are listed in Table 3-1. Because the dipole field of the H_2O molecule is strong, the surface electronic structure should be affected as shown in Figures 3-2 to 3-4. Secondly, after adding more H_2O molecules over the surface of LAO/STO, some H_2O molecules are at high electrical potential which results in a significant increase of 2DEG.

Since the work function is determined by the difference of Fermi-level and the potential of the vacuum above the top surface, it should be sensitive to the polar

direction of polar molecules when the molecules are placed between the vacuum and the top surface of the film, as shown in Table 3-1.

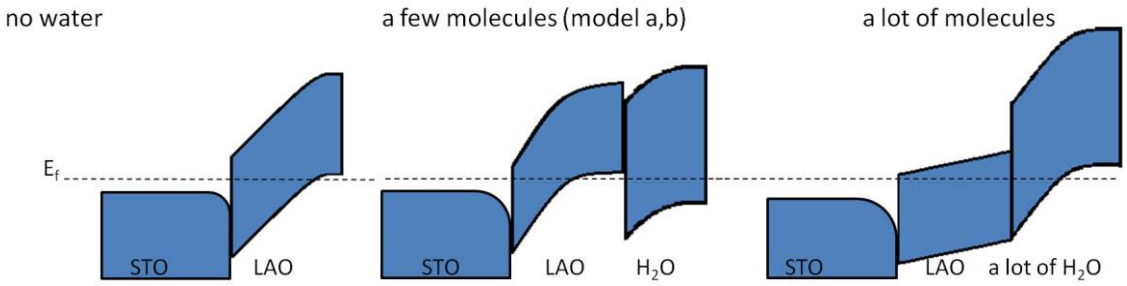

Figure 3-6 Sketching band structure along z for no water (left), few water (middle) and lots of water (right)

Figure 3-6 shows the band structure diagram with water adsorbates outlined from PDOS. With the presence of few H_2O molecules, the valence band rises in deeper layers of LAO, as shown in the middle of Figure 3-6 (b), but it may be depressed on the surface. The energy levels of the H_2O molecules depend on their orientations, but the energy of the valence electrons of H_2O is not high enough to reach the Fermi-level, so 2DEG at LAO/STO interface should be contributed only from LAO. From the results of calculation, density of 2DEG and holes increase with the presence of more H_2O on surface. When the electrical potential energy at H_2O molecules increases, the energy of valence electrons of H_2O may reach Fermi-level. Therefore, the valence electrons of the upper H_2O are of high energy and are transferred to interface of LAO/STO, and thus the increase of 2DEG conduction can be observed [21]. Since the conduction band with H_2O shown in Figure 3-2 is almost unchanged with H_2O, it is suggested that the mobility should not vary significantly and the conductance change should be

proportional to the change of conduction electron density. This has been proved by experimental results [21].

The change of work function is also determined in Table 3-1. The great change of electron density and the work function, but the conduction band at the interface varies little after adding H_2O molecules with a few molecules. It suggests that the change of transport properties reported [21, 22]may also be related to the change of conduction electron density or the change of work function.

When polar molecules (H_2O) cover part of the surface of LAO/STO, a Schottky junction may be formed between the covered part and the uncovered part as suggested in ref [22]. The formation of Schottky junction should be determined by the difference of work function between two regions and the carrier density of these two regions. Since the depletion layer is shortened for higher carrier density, and it is too thin to stand in conventional metals. Although the conduction of LAO/STO interface is known as metallic (around 0.05 electrons per 1×1 surface, mostly distributed within several units of STO below the interface), the concentration of the conduction electrons is much lower than conventional metals (several electrons per ion). For models a and b, the change of work function is small; however, for models c with very strong polarization of H_2O, the 2DEG work function increases significantly and the Schottky junction can be formed. This result sheds light on the nature of formation of a Schottky junction in a few reported experimental results, and also predicts that such effect can be used for field effect transistor devices based on the LAO/STO 2DEG.

3.4 Conclusion

Adsorption of H_2O molecules on AlO_2-terminated surface of $LaAlO_3/SrTiO_3$ heterostructure has been investigated by first-principles. It reveals that adsorption of polar water molecules on the surface of $LaAlO_3$ can remarkably enhance the carrier density of two-dimensional electron gas at the interface. The resultant large change of the work function may induce the formation of a Schottky junction inside the 2DEG layer. This change raises the possibility in various applications, such as polar molecule sensors.

CHAPTER 4 ELECTRONIC PROPERTIES OF (110) $LaAlO_3/SrTiO_3$

4.1 Introduction

When LAO layer is epitaxially grown beyond a critical thickness of 4 unit cells, on (001) STO with TiO_2-terminated surface, the interface of LAO/STO becomes metallic conducting [6-8]. This can be explained by the model of polar catastrophe [6-8]. In terms of the ionic charge, LAO consists of alternating polar layers of $(LaO)^+$ and $(AlO_2)^-$ along [001] direction, but STO consists of neutral layers of (SrO) and (TiO2). Electronic reconstruction occurs at $(LaO)^+$ / (TiO_2) interface for the compensation of polar discontinuity between polar LAO and nonpolar STO in the model of polar catastrophe. Consequently 0.5 e per two dimensional unit is required to compensate as expected in the model of polar catastrophe.

However, recent experimental work has found 2DEG in systems different from the epitaxial LAO thin film on (001) STO [24, 25, 65]. The reports shows that to obtain metallic conduction at LAO/STO interface, the epitaxial LAO thin film on (001) STO is not a must; the surface of the STO can also be (110) or (111) [25], and the LAO film can even be amorphous [24, 65]. Herranz, *et al.* [25] have reported the observation of high-mobility conduction at (110) and (111) LAO/STO interfaces. Polar discontinuity should not occur at the (110) interface of LAO/STO, since LAO consists of stacks of

$(LaAlO)^{4+}$ and $(O2)^{4-}$, while STO is $(SrTiO)^{4+}$ and $(O2)^{4-}$. Therefore in this chapter, theoretical investigation has been carried out on the transport properties of (110) LAO/STO interface by first principles calculation.

4.2 Computation Details

First principles calculation is achieved by Vienna ab initio Simulation Package (VASP) in the frame of Density Functional Theory (DFT) with local density approximation (LDA). The cut-off energy of plane wave basis is 500eV and the k-point meshes are 11×7×1. All structures are relaxed till the force on each atom is less than 0.02eV/ Å. Since experiments [25] show that the (110) STO surface can be atomically flat and thin film can be obtained with epitaxial growth, surface (interface) reconstruction is not considered. The (1×1) superlattices (SL) $(LaAlO_3)m/(SrTiO_3)n$ are constructed with various number of monolayers (MLs) of LAO and STO (m and n) and the structure of $(LaAlO_3)_6/(SrTiO_3)_6$ SL is shown in Figure 4-1. A stoichiometric SL of $(LaAlO_3)m/(SrTiO_3)n$ has two same interfaces with the stacking of $(LaAlO/O_2/SrTiO)$. N-type or p-type doped SLs were also studied with doped interfaces $(LaTiO/O_2/SrTiO$ for n-type and $SrAlO/O_2/SrTiO$ for p-type). For the doped SLs, the bottom layers remain unchanged, i.e. forming an undoped interface $(LaAlO/O_2/SrTiO)$.

The x, y, and z axes are laid into [1 0 0], [0 1 0] and [0 0 1] directions of STO lattice, respectively. The theoretical value of STO and LAO lattice constants are a_{STO} = 3.86 Å and a_{LAO} = 3.74 Å. The lattice constants are set to $a_{SL} = a_{STO}$, $b_{SL} = \sqrt{2}\ a_{STO}$ and

$c_{SL} = m/\sqrt{2}\ a_{LAO} + n/\sqrt{2}\ a_{STO}$ for SL of $(LaAlO_3)m/(SrTiO_3)n$.

4.3 Results and Discussion

4.3.1 Intrinsic (110) $LaAlO_3/SrTiO_3$ Interface

The transport properties of the intrinsic (110) LAO/STO SL are investigated. The SL with m=6, and n =6 are shown in Figure 4-2. The sum of unit (m+n) is varied, but the results are similar. Spin-polarized calculations are also tried for this heterostructure system and the results (e.g. the total density of states as shown in Figure 4-1) indicate that all models are non-magnetic.

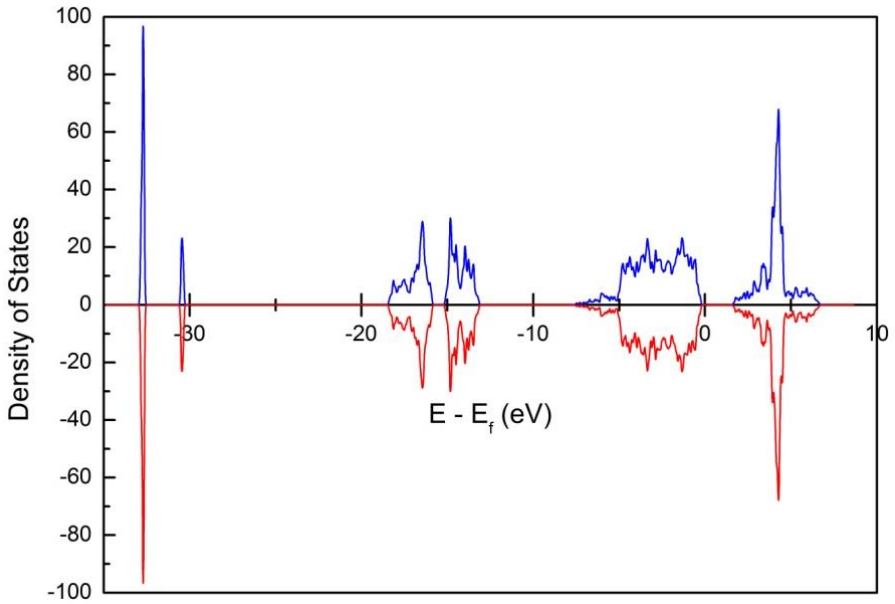

Figure 4-1 Total density of states (Total DOS) of (110) LAO/STO SL, positive for spin up and negative for spin down

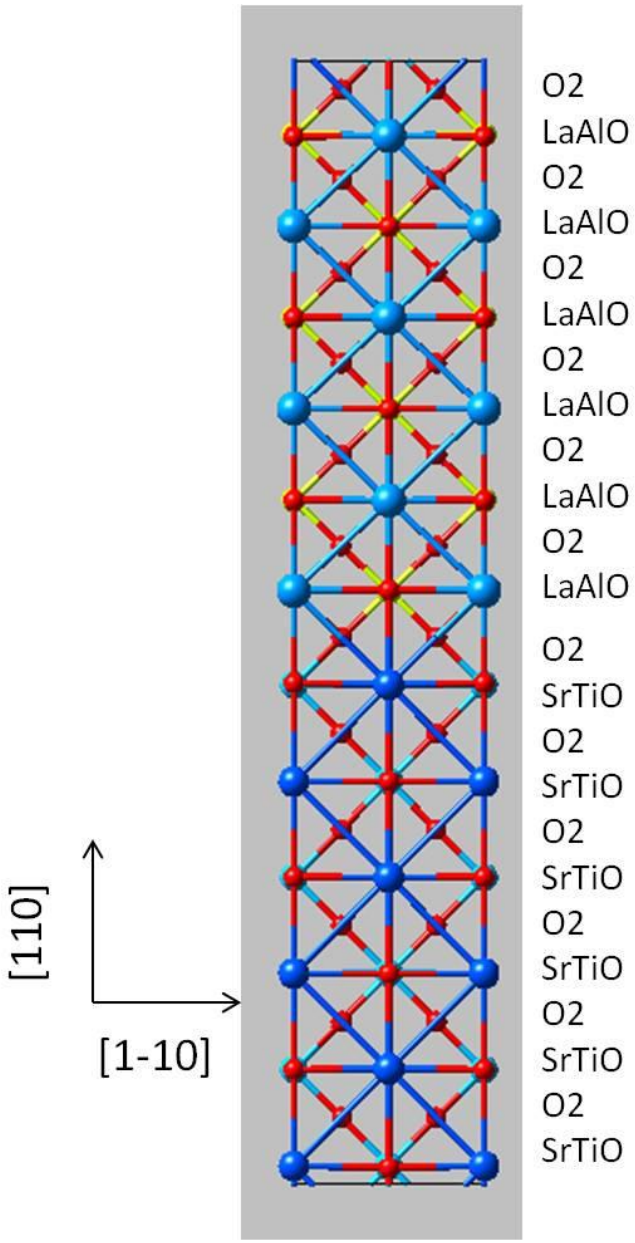

Figure 4-2 Structure of $(LaAlO_3)_6/(SrTiO_3)_6$ superlattice (SL). Large light-blue balls represent La, deep-blue balls are Sr, yellow balls are Al, small light-blue balls are Ti, and red balls are O.

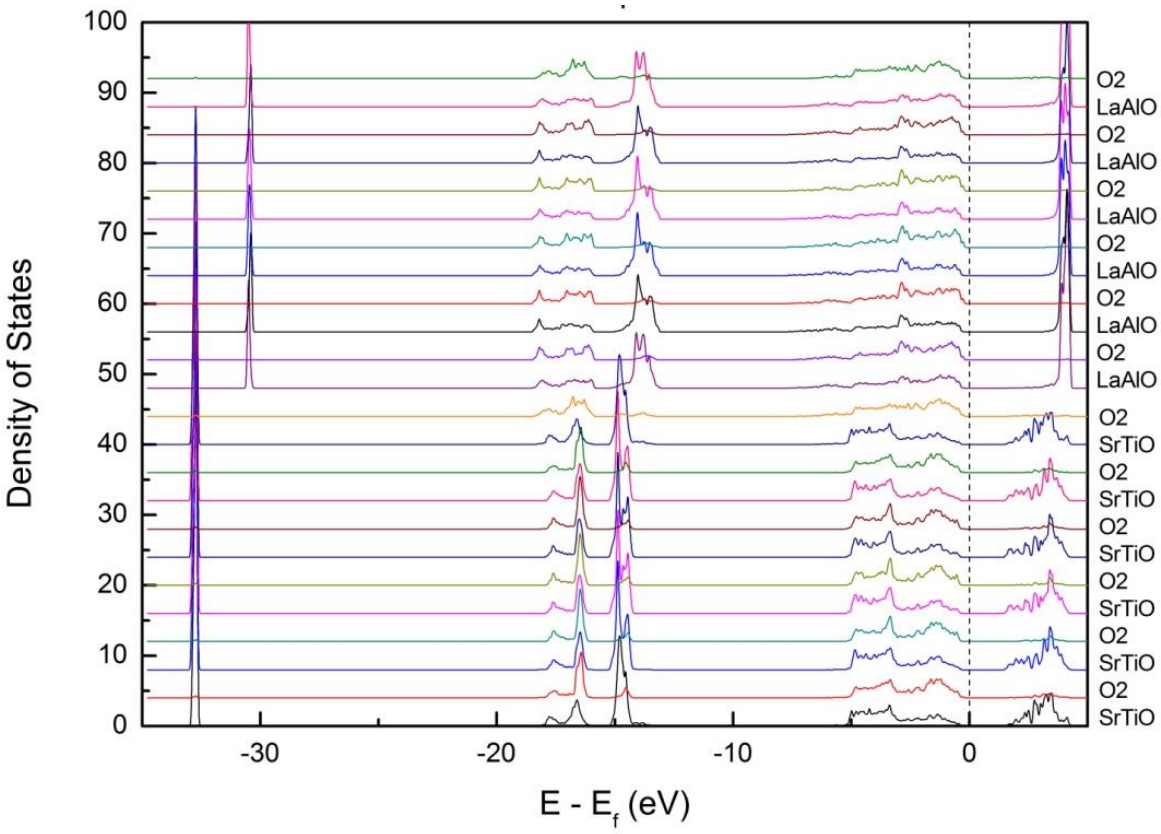

Figure 4-3 Layer-density of states (LDOS) of LAO_6/STO_6 SL

The calculated layer-density of states (LDOS) of (110) LAO_6/STO_6 SL is shown in Figure 4-3. As expected, without polar discontinuity, the peaks of O 2s orbitals at different layers remain at about -17eV. This indicates that the electric field (electrical potential gradient) along [110] vanishes, since there is no polar discontinuity at the (110) interface of LAO/STO. Band gap is 1.76 eV for the LAO_6/STO_6 SL, which is close to the STO band gap obtained in LDA calculation. Therefore, the stoichiometric (110) LAO/STO interface should be insulating, and the conducting (110) LAO/STO interface in experiment [25] should be non-stoichiometric interface. Doping might present in the non-stoichiometric (110) LAO/STO interface, and therefore effect of doping is studied in the following section.

4.3.2 N-Type/ P-Type Doping

In order to study the transport properties reported in ref [25], the conduction due to doping at interface is considered. N-type doping can be achieved by replacing an Al by Ti (or equivalently replacing Sr by La), and the layer LaTiO with an extra electron would be obtained at the heterostructure. Similarly, p-type doping can be modeled by replacing an La by Sr (or equivalently replacing Ti by Al), and the layer SrAlO with an hole would be obtained.

The spatial band structure of n-type SL can be sketched by layer-density of state (LDOS) as shown in Figure 4-4 (a). For n-type doped SL, a peak of LDOS corresponding to conduction band acrossing Fermi level at the doped interface (LaTiO layer), and the peak rises in the next two monolayers from interface, but it becomes shorter in deeper layers of SrTiO in STO as shown in Figure 4-4 (b). Electrons are not strongly confined at interface, but they distribute mostly at the second monolayer in STO from the doped interfaces. It is different from the 2DEG at (001) LAO/STO heterostructure, where most 2DEGs confined at the interface layer.

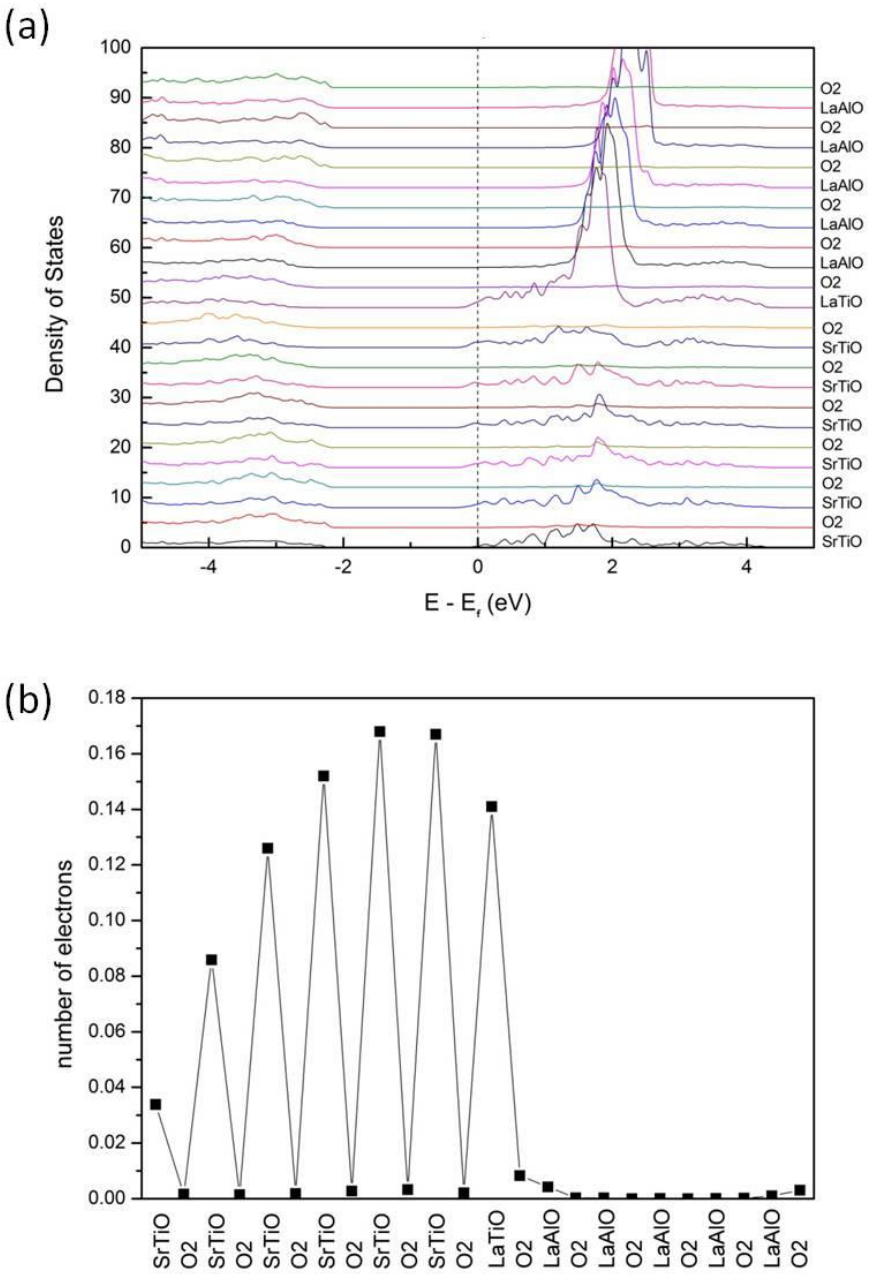

Figure 4-4 (a) Layer-DOS of n-type $(LAO)_6/(STO)_6$ SL, and (b) distribution of electrons in n-type SL.

As shown in Figure 4-5 (a), for p-type doped SL, Fermi-level shifts to valence band; while holes distribute mostly at the O_2 layers in LAO as shown in Figure 4-5 (b).

Unlike the distribution of electrons, most holes distribute in the layer of interface with the acceptor (layer of SrAlO) and the layers next to it.

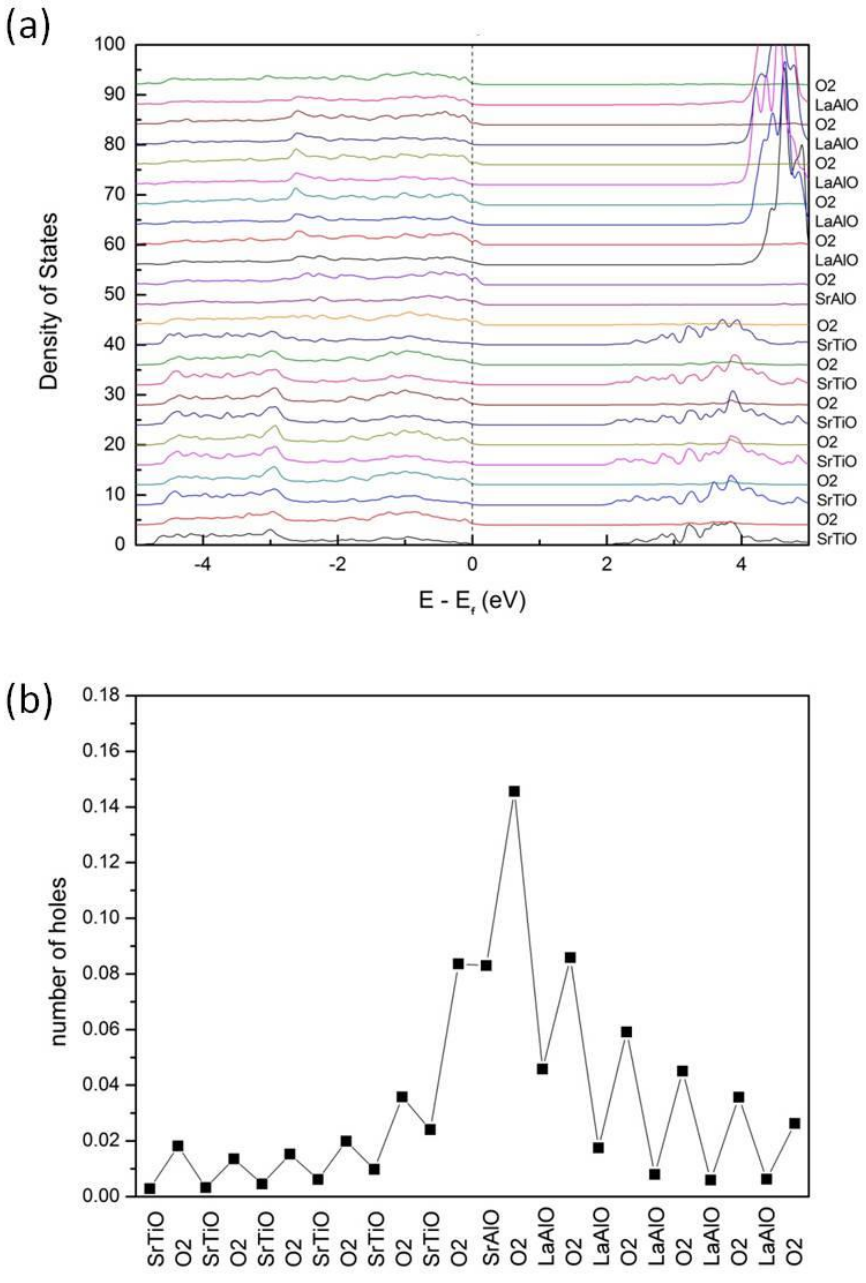

Figure 4-5 (a) Layer-DOS of p-type $(LAO)_6/(STO)_6$ SL, and (b) distribution of holes in p-type SL.

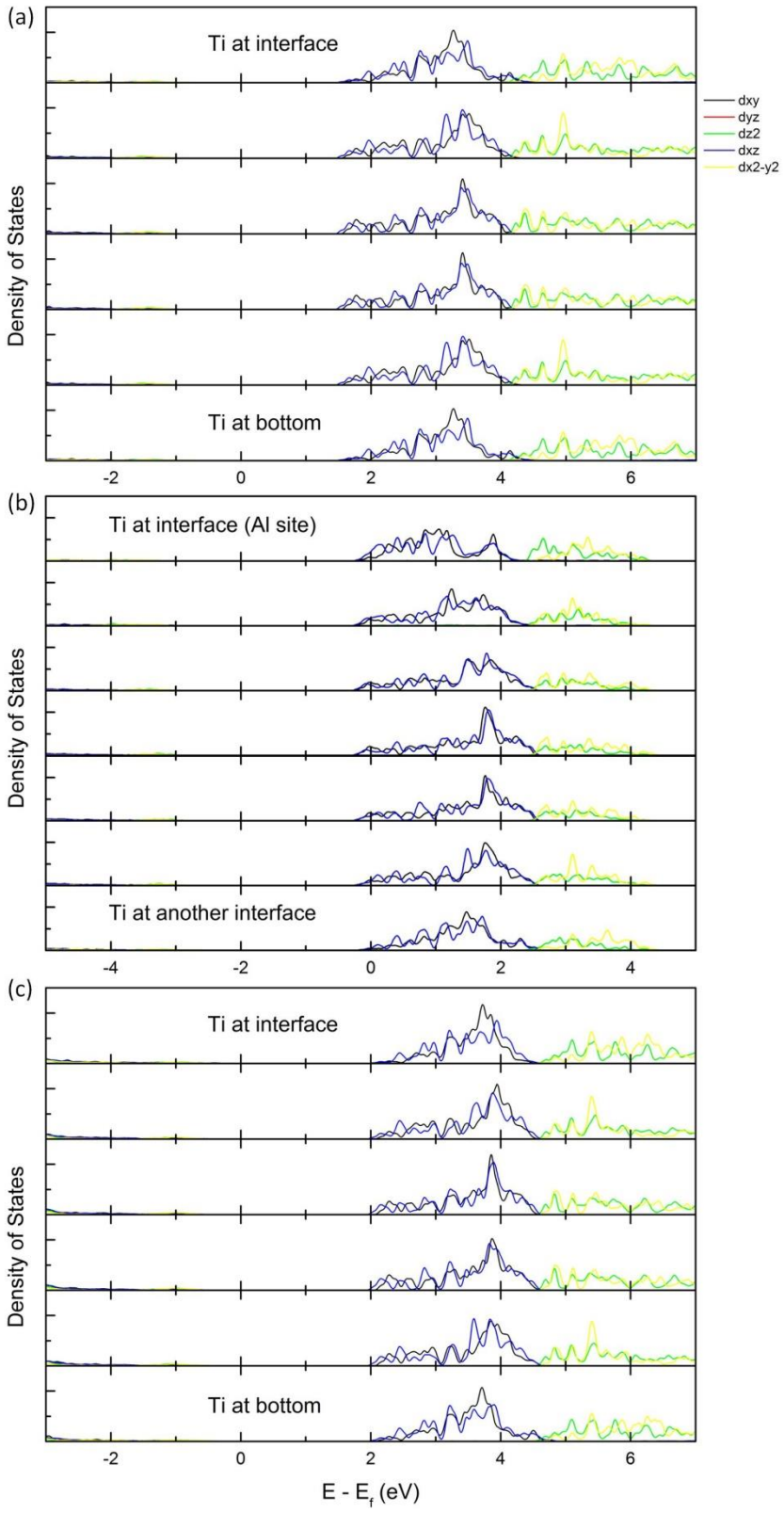

Figure 4-6 PDOS of Ti in (a) intrinsic, (b) n-type doped and (c) p-type doped $(LAO)_6/(STO)_6$ SL of. It should be noted that the scale is shifted for Figure 4-5 (b).

Figure 4-6 shows the PDOS of Ti for the intrinsic, n-type and p-type doped SL. One can see that they are basically similar, but all peaks shift in energy for the n-type and p-type doped SL correspondingly, since doping may change the chemical potential of electrons.

The peaks of the states of Ti d_{yz} and d_{xz} are completely overlapped, and these orbitals are equivalent under the symmetry at the (110) interface. Ti d_{xy}, d_{yz} and d_{xz} belong to the t_{2g} orbitals. Ti d_{z2} and d_{x2-y2} are the e_g orbitals. It can be seen that Ti d orbitals are split into e_g with higher energy and t_{2g} with lower energy as expected in crystal field theory, but e_g state is of less interest because it should not affect the conduction due to its high energy. However, the t_{2g} orbital further splits into a slightly higher energy state (d_{xy}) and two degenerated states at lower energy in the (110) interface. At both (001) and (110) interfaces of LAO/STO, the t_{2g} orbitals are further split, but the order of t_{2g} states in energy is reversed that the energy of d_{xy} is lower than those of d_{yz} and d_{xz} at (001) interface. The t_{2g} states will be studied later in this report.

In Figure 4-7, band structure of the (110) interface of LAO/STO SL is shown. It can be seen that the Fermi-level E_f moves to E_{fn} with n-type doping, and E_{fp} with p-type doping, but the band gap remains. One can also see that there is no in-gap states. At Γ point, there are several sets of bands (each set has three bands) located in the region of conduction band, and each set should be contributed by t_{2g} states of Ti at different layers in STO. The set of bands with the lowest energy in the conduction band are contributed by t_{2g} states of Ti located at 3 to 4 monolayers away from the interfaces, and the states of the set of the next lowest energy should be contributed by t_{2g} states of Ti located

within about 2 monolayers from the interfaces. The three bands in each set have different curvatures around Γ point which are similar to the case of (001) LAO/STO with the flatten Ti d_{xz} bands along y direction and steeper Ti d_{xy} and d_{yz} bands. The band structure is in consistence with some points suggested by Chen and Balents [95]. For example, t_{2g} of (110) oxide STO interface further splits into three non degenerate orbitals, which becomes a d_{xy} orbital and two hybrid orbitals of d_{yz} and d_{xz}. In ref [95], however, the t_{2g} bands are also suggested to be two quasi-one-dimensional bands in higher energy and a two-dimensional band in lower energy at their band bottoms. In the calculated band structure in Figure 4-7 the d_{xy} band is localized (flatten) along Γ-Z and the two combinations of d_{yz} and d_{xz} are localized along Γ-X. In other words, all of these t_{2g} bands should be quasi-one-dimensional.

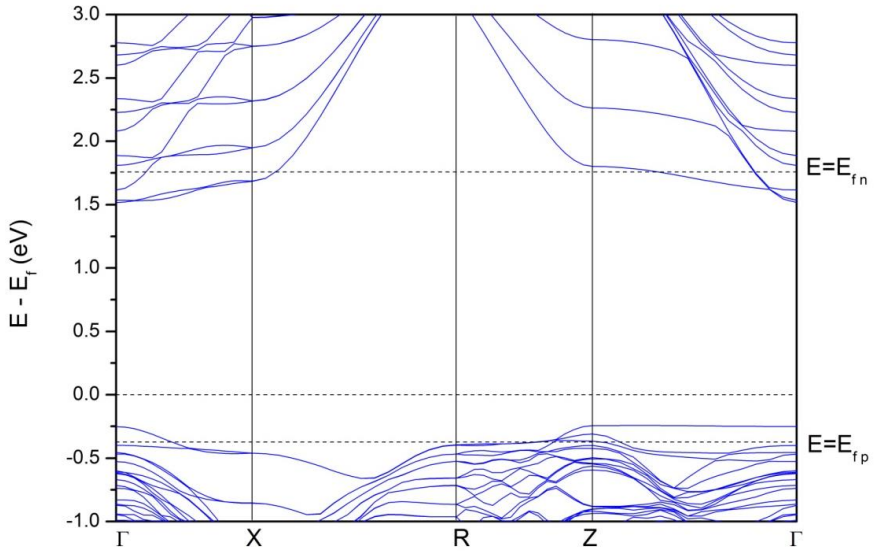

Figure 4-7 Band structure of LAO_6/STO_6 SL in the plane Brillouin Zone parallel to (110) interface, in terms of reciprocal lattice vectors with points Γ(0,0), X (0, 1/2), R(1/2,1/2) and Z(1/2, 0)

4.3.3 Oxygen Vacancy Effect

In order to find the oxygen vacancy effect to the interface transport properties, (110) oriented SL with oxygen vacancy (OV) is also studied. To prevent OV cluster, only OV at O_2 layer is considered. OVs at several sites which are denoted by V_0, V_1 and V_{-1} have been calculated, where V_0 (the interface), V_1 (1 monolayer above interface in LAO) and V_{-1} (1 monolayer below interface in STO).

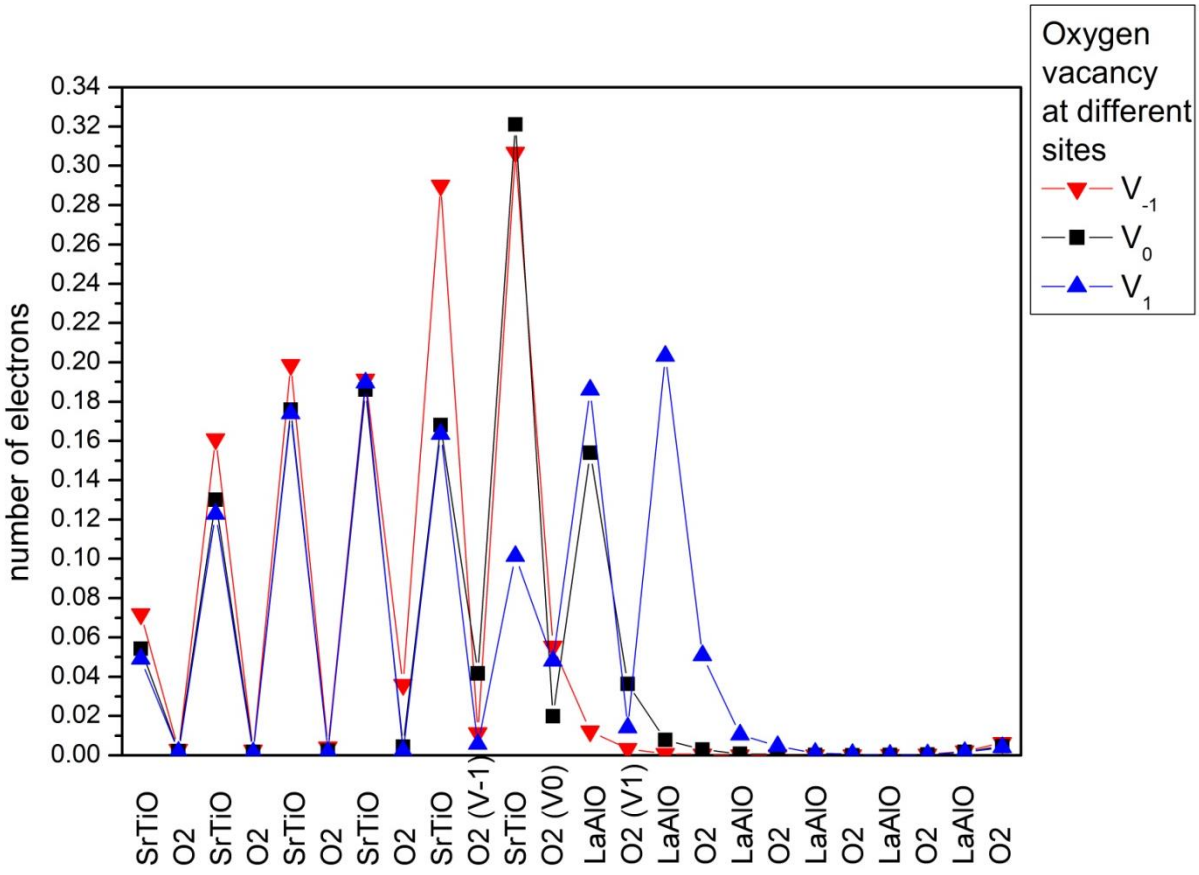

Figure 4-8 Distribution of electrons in SL with OV at different sites.

An OV is equivalent to 2 extra electrons doped in the LAO/STO SL. In Figure 4-8, some electrons are located around the OV, but most electrons spread to the SrTiO layers in STO. The distribution of electrons in STO away from OV is similar to those of n-type doped SL as shown in Figure 4-4 (b), and it depends little on the location of OV. This suggests that some extra electrons are localized around the site of oxygen vacancy (OV), while some are spreading in STO as n-type dopant. It should also be noticed that the sum of the conduction electrons at each layer is less than 2, since the number of electrons is evaluated by Layer-DOS which requires the projection within spheres centered at nuclei on the same layer.

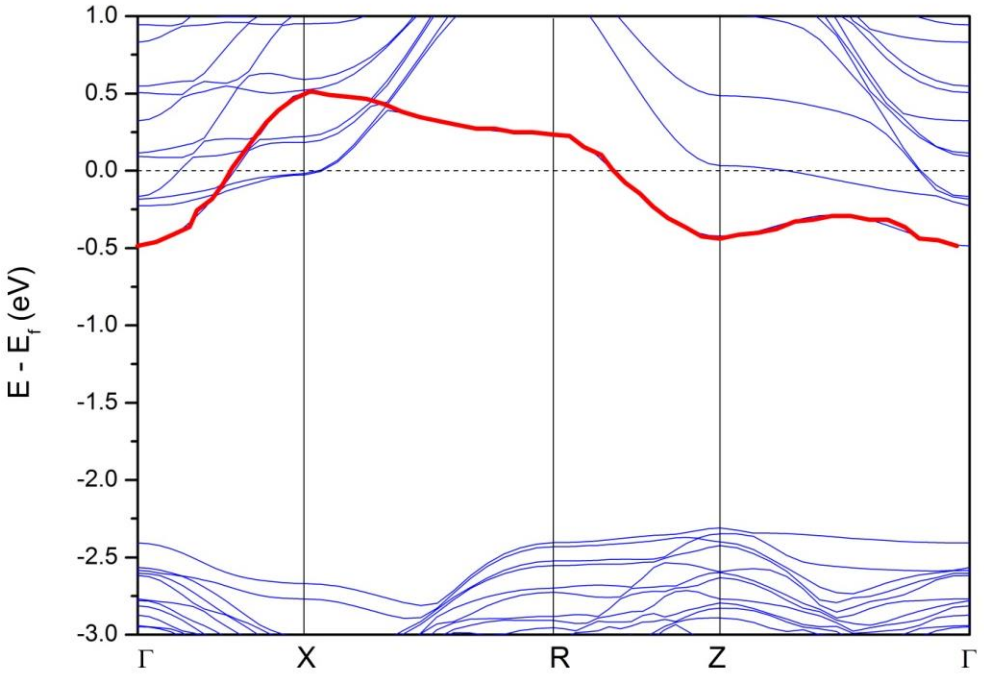

Figure 4-9 Band structure of the (110) LAO/STO SL with OV at site V_1, the additional band is highlighted in red.

Band Structure of (110) SL with OV at site V_1 is shown in Figure 4-9 and

similar results have been observed with OV at the other sites of V_{-1} and V_0. With the presence of oxygen vacancy (OV) in STO or LAO, an additional band appears in the bottom of conduction band. The additional state with oxygen vacancy has also been reported in theoretical studies of $SrTiO_3$ [96, 97], (001) surface of $SrTiO_3$ [97] and (001) interface of $LaAlO_3/SrTiO_3$[98]. This state is partially contributed by the e_g orbitals for the systems with OV at V_{-1} and V_0. It should be noticed that the density of OV in our calculation is very high (1 OV per 1×1 unit), and the band due to OV should be more localized at lower density of OV [97]. The conductivity therefore should be contributed by the t_{2g} orbitals.

The 2DEG at (001) LAO/STO is believed to be driven by the polar discontinuity at the interface, and the conduction electrons are contributed by three components of reconstructed Ti d orbitals, where most of them are at Ti d_{xy} and little at Ti d_{yz}/d_{xz}. The first one is lower in energy and strongly confined within several layers of STO from the interface, but the second one distributes deeper in STO. Most of the conduction electrons should occupy the d_{xy} orbitals and produce 2-dimensional isotropic conduction at the n-type (001) LAO/STO interface.

In comparison to (001) LAO/STO, polar catastrophe at stoichiometric (110) LAO/STO is not expected to occur and produce the conduction state, since it has no polar discontinuity along [110]. However, oxygen vacancy or other electron source may produce n-type doped interface. Most recently, Annadi, *et al.* [99], suggested that the buckled LAO/STO (110) interface may cause the polar-catastrophe. In such a model, STO is believed to have a non-stoichiometric (110) surface which can be regarded as a

SrTiO- terminated surface with Sr site vacancies. La is placed on Sr vacancy when LAO is deposited on STO, and the interface consists of a stacking of $LaAlO/O_2/LaTiO/O_2/SrTiO$. It should be noticed that the n-type doped SL in this report also have the interface of $LaAlO/O_2/LaTiO/O_2/SrTiO$. It implies the results obtained in this thesis may also be suitable for the model of buckled interface.

The t_{2g} orbitals at (110) LAO/STO consists of a d_{xy} state and two hybridized states of d_{yz} and d_{xz} . As shown in Figure 4-9, the energy of d_{xy} is higher than the energy of the other two t_{2g} bands. It can be expected that the conduction electrons at (110) LAO/STO, if they exist or are produced by doping such as oxygen vacancies, would be more localized along [1 -1 0] but less localized along [0 0 1]. The in-plane conduction therefore should be anisotropic.

4.4 Conclusion

In conclusion, the electronic structures at (110) LAO/STO interface have been investigated by first principles. The conduction at (110) interface, if exists due to doping or other sources, should be contributed by Ti t_{2g} orbitals which also contribute to the 2DEG at (001) LAO/STO. However, the distribution and the transport properties of the conduction electrons should be different from those at (001) LAO/STO. The in-plane conduction at (110) LAO/STO should be anisotropic.

CHAPTER 5 ELECTRONIC PROPERTIES OF (111) $LaAlO_3/SrTiO_3$

5.1 Introduction

Similar to the calculation of (110) $LaAlO_3/SrTiO_3$ (LAO/STO) in Chapter 4 of this thesis, the first principles calculation was also carried out for (111) LAO/STO heterostructure.

Recent reports show that epitaxial growth of LAO thin film on (001) STO is not necessary for interfacial conduction, i.e. the surface of STO can also be (110) or (111) [25], instead of (001). High mobility conduction was observed at (110) and (111) interfaces of LAO/STO, when the LAO is beyond certain thicknesses [25]. Unlike (110) LAO/STO in Chapter 4, polar discontinuity, similar to (001) LAO/STO heterostructure, should occur at the (111) interface, since along [111] direction, STO consists of layers of $(SrO_3)^{4-}$ and $(Ti)^{4+}$, and LAO consists of layers of $(LaO_3)^{3-}$ and $(Al)^{3+}$. Therefore 0.5 e per two dimensional unit is expected to compensate as in the model of polar catastrophe. However, there has not been any theoretical study on transport properties and electronic structures of (111) LAO/STO heterostructure yet. Therefore the transport properties and electronic structures of (111) LAO/STO interface are investigated theoretically in this chapter.

5.2 Computation Details

First principles calculation is achieved by Vienna ab initio Simulation Package (VASP) in the framework of Density Functional Theory (DFT) with local density approximation (LDA). The cut-off energy of plane wave basis is 500eV and the k-point meshes are 7×7×1. All structures are relaxed till the force on each atom is less than 0.02eV/ Å. Since experiments[25, 100, 101] show that the (111) surface of STO can be atomically flat and thin film can grow epitaxially, surface (interface) reconstruction is therefor not considered, and models are built to have atomic flat interfaces. The (1×1) superlattices (SL) $(LaAlO_3)_m/(SrTiO_3)_n$ are constructed with various numbers of monolayers (ML) of LAO and STO (m and n), and the structure of $(LaAlO_3)_6/(SrTiO_3)_6$ SL is shown in Figure 5-1. A stoichiometric SL of $(LaAlO_3)m/(SrTiO3)_n$ has two different interfaces, LaO_3/Ti and SrO_3/Al, but it can also be changed into both LaO_3/Ti (or both SrO_3/Al) by replacing Al by Ti at SrO_3/Al (or replacing La by Sr at LaO_3/Ti). This provides one additional electron (hole) per SL.

The x, y, and z axes are laid into [1 0 0], [0 1 0] and [0 0 1] directions of STO lattice, respectively. The theoretical lattice constants of STO and LAO are a_{STO} = 3.86 Å and a_{LAO} = 3.74 Å. The lattice constants of the superlattice are set to $a_{SL} = b_{SL} = \sqrt{3}\ a_{STO}$ and $c_{SL} = m/\sqrt{3}\ a_{LAO} + n/\sqrt{3}\ a_{STO}$ for the $(LaAlO_3)_m/(SrTiO_3)_n$.

5.3 Results and Discussion

5.3.1 Relaxation of Atoms at (111) $LaAlO_3/SrTiO_3$ Interface

Similar to the study in Chapter 4, the transport properties and electronic structures of intrinsic (111) LAO/STO heterostructure were investigated first. It is worthy noting that relaxation of atoms may affect the electronic properties of the system, especially the formation of 2DEG in polar-catastrophe model, since it may reduce the internal electric field due to polar discontinuity at interface. For the doped systems, the conduction is caused by the dopant atoms. Therefore, relaxation of atoms is studied only at the intrinsic (111) LAO/STO interface.

The model of SL with m=6 and n =6 is shown in Figure 5-2. It should be noticed that in the models of SLs, the sum of unit (m+n) and the ratio between m and n (m/n) are varied, but the results from different variants are similar, so only the models of m=6 and n=6 are shown in this report.

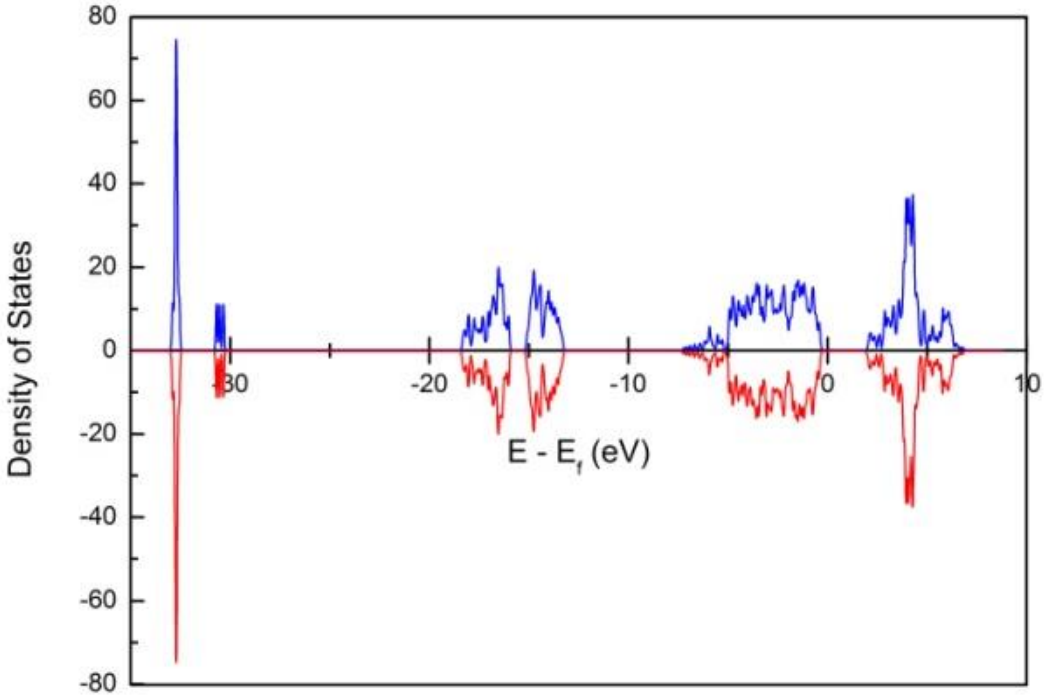

Figure 5-1 Total density of states (TDOS) of (111) LAO/STO SL, positive for spin up and negative for spin down.

Spin-polarized calculations are also performed and the results indicate that all models in this report are non-magnetic. It can be reflected by the total density of states as shown in Figure 5-1, since the density of states are the same for spin up and spin down.

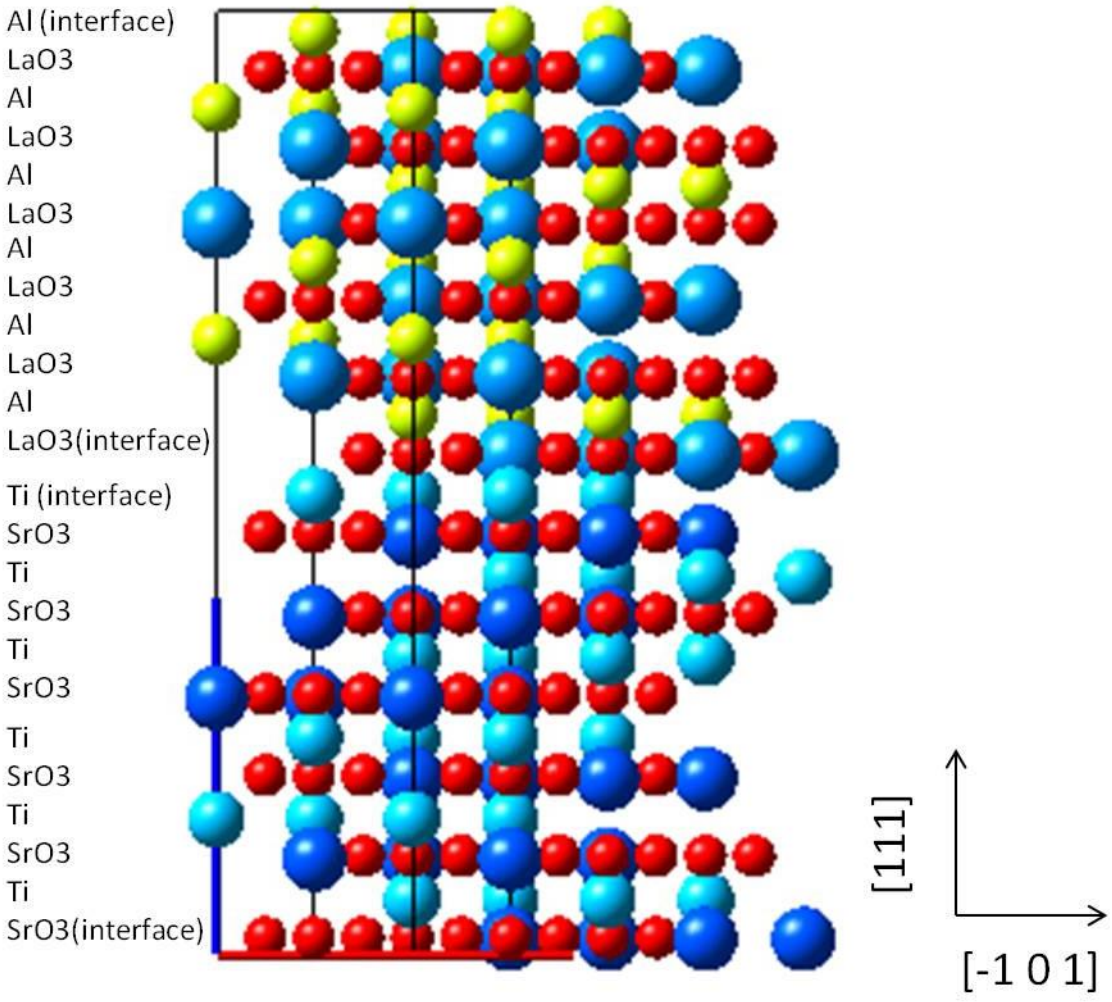

Figure 5-2 Structure of (111) $(LaAlO_3)_6/(SrTiO_3)_6$ superlattice. Large light-blue balls represent La, deep-blue balls are Sr, yellow balls are Al, small light-blue balls are Ti, and red balls are O.

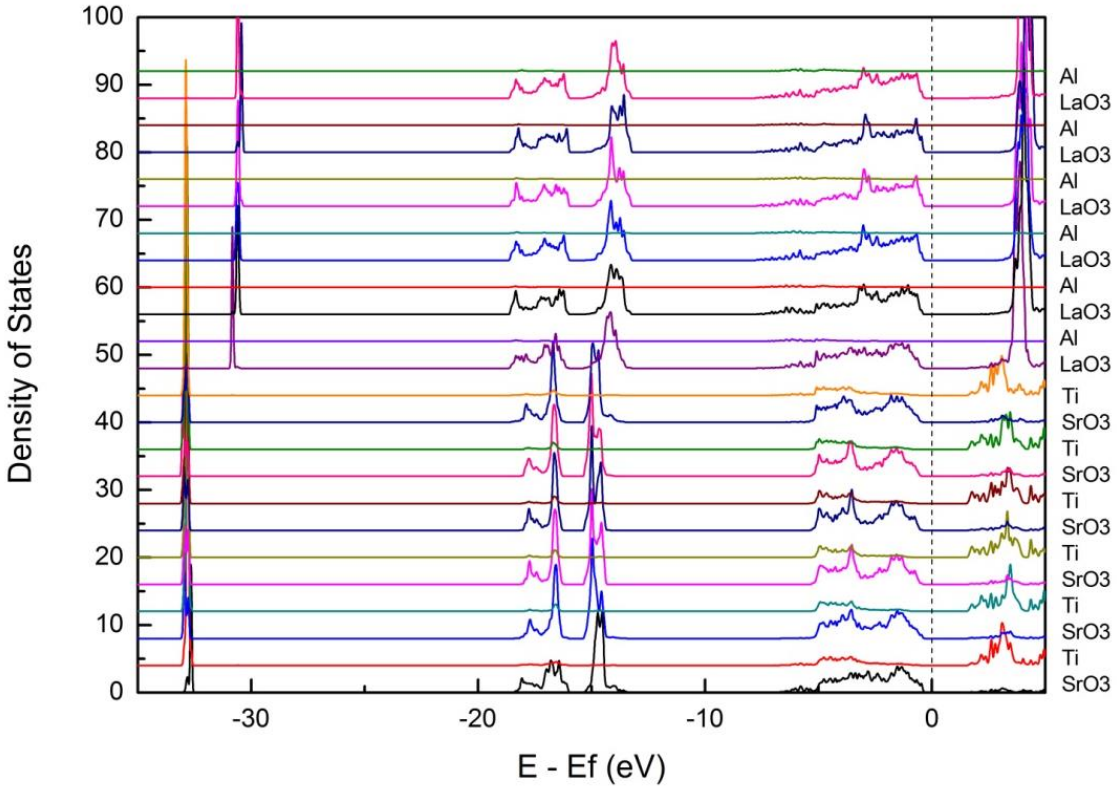

Figure 5-3 Layer-DOS of (111) $(LAO)_6/(STO)_6$ with relaxation

Figure 5-3 shows the layer-DOS, where the peaks at about -18eV are contributed by O 2s orbitals at different layers, and these peaks are almost located at the same energy, indicating that the potential varies little in different layers of SL and the internal electric field due to polar discontinuity is not observed. The band along [111] is flat, unlike the zigzag-like band along [001] in LAO and STO of (001) LAO/STO SL as shown in ref. [102] or the sloped band of (001) LAO thin film in ref. [47]. Band gap of 1.95 eV is obtained in $(LAO)_6/(STO)_6$ which is close to the band gap of STO in LDA calculation. This suggests that the band gap at the (111) LAO/STO interface is unlikely reduced as those in (001) LAO/STO.

The absence of polar discontinuity effect in Figure 5-3, which appears in (001)

LAO/STO heterostructure, is unexpected. Our study suggests that relaxation of atoms may partially compensate the polar discontinuity which has been ascribed as the origin of 2DEG in the (001) LAO/STO heterostructure. In Figure 5-4, the polarization due to relaxation of atoms along the out-of-plane direction [1 1 1] is estimated via the equation $\Delta P = \frac{e}{\Omega}\sum_i Z_i \times \Delta u_i$, where Z_i is the Born effective charges, u_i is the displacement for atom i. Effective charges are given in ref [103] for LAO and ref [104] for STO. Average polarization due to relaxation is -0.0269 e/ Å^2 (0.432 C/m^2) in STO and 0.0026 e/ Å^2 (0.042 C/m^2) in LAO. From the equation $P_{LAO} - P_{STO} = \sigma_{interface}$, it equivalently compensates 0.38e per 1×1 unit of interface which is close to the full compensation by 0.5e per interface unit in the ionic limit.

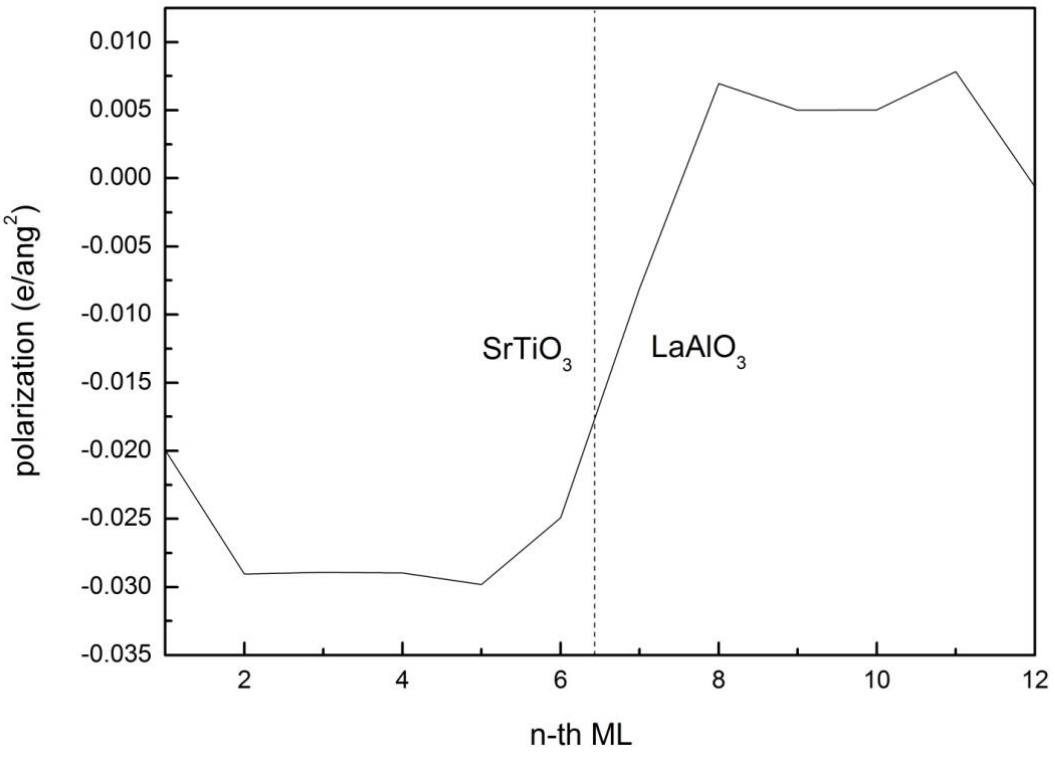

Figure 5-4 Polarization due to relaxation along [111] at different monolayer (ML)

However, as shown in Figure 5-5, when the relaxation of atomic position is restricted (an hypothetic model), zigzag-like band along [111] of (111) LAO/STO SL can be obtained and conduction electrons appear. Therefore, the significance of the polar discontinuity effect (and the resulting conduction) depends on how much the atoms relax.

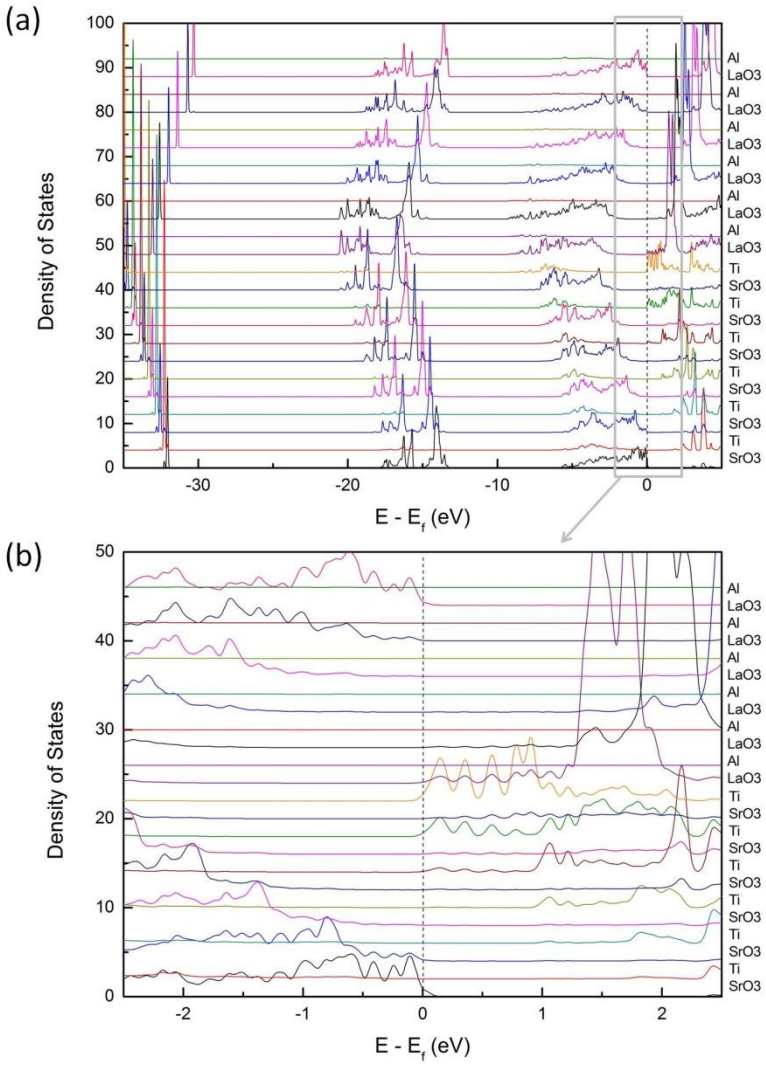

Figure 5-5 (a) Layer-DOS of $(LAO)_6/(STO)_6$ without relaxation, and (b) enlarged (a) in the range (grey rectangular) in around Fermi-level .

5.3.2 N-Type/ P-Type Doping

N-type (p-type) doping has been modeled by replacing an Al (La) by Ti (Sr) at the interface and the corresponding SLs have both LaO3/Ti (SrO3/Al) interfaces. The spatial band structure can be sketched by layer-density of state (LDOS). LDOSs of the n-type interface and p-type interface remain unchanged but with Fermi-level shifted from the undoped systems. As shown in Figure 5-6, for n-type doped SL (Ti on Al site at one interface), electrons distribute away from interface in STO. It is unlike the 2DEG at (001) LAO/STO heterostructure, where most 2DEG is confined at the interface layer. The electron distribution at (111) LAO/STO however is similar to that of (110) LAO/STO as shown in Figure 4-4.

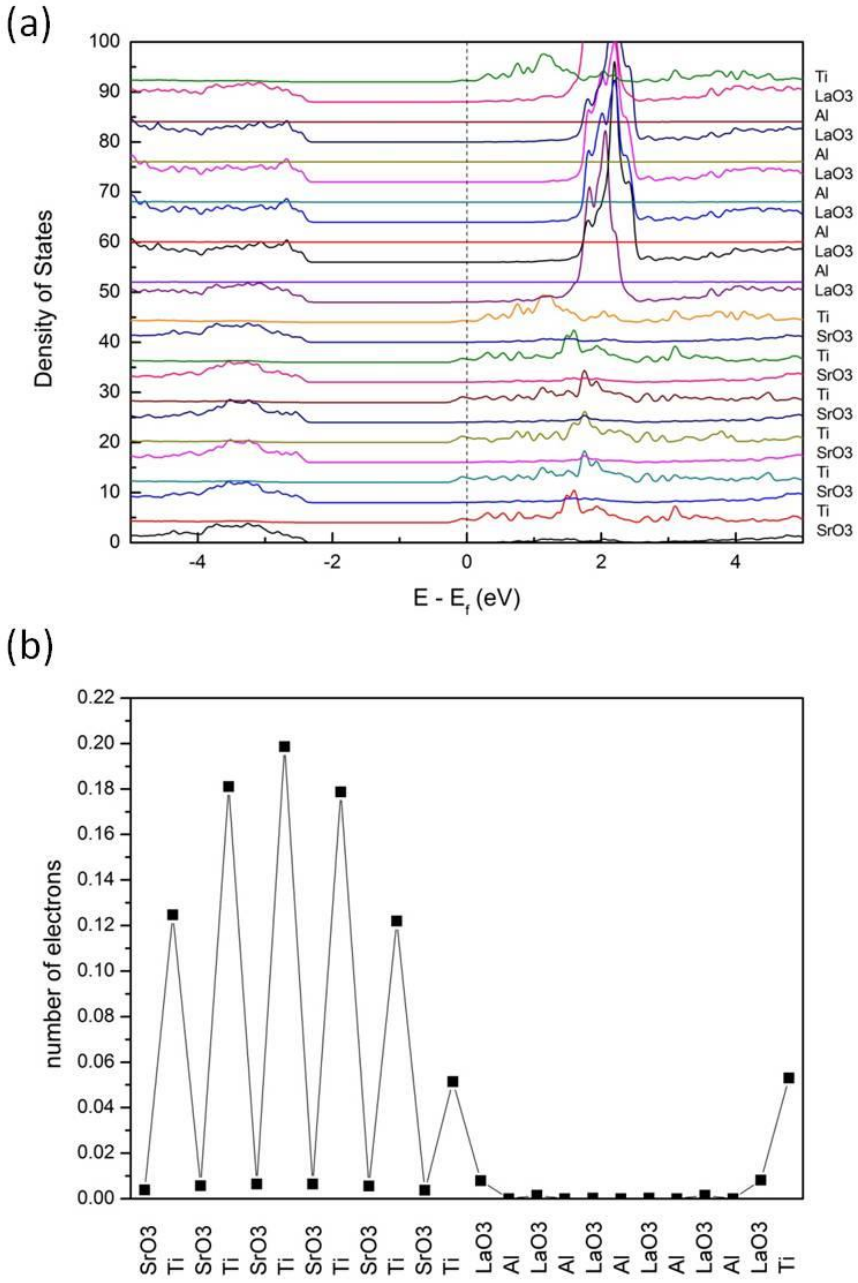

Figure 5-6 (a) Layer-DOS of n-type (111) $(LAO)_6/(STO)_6$ SL, and (b) distribution of electrons in n-type SL.

For p-type doped SL (Sr replace La) the Fermi-level shifts to valence band as shown in Figure 5-7(a). Holes distribute at O of each layer of SrO_3 and LaO_3 in the SL

as shown in Figure 5-7(b), but most holes locate at LaO_3 layers next to the SrO_3/Al interfaces.

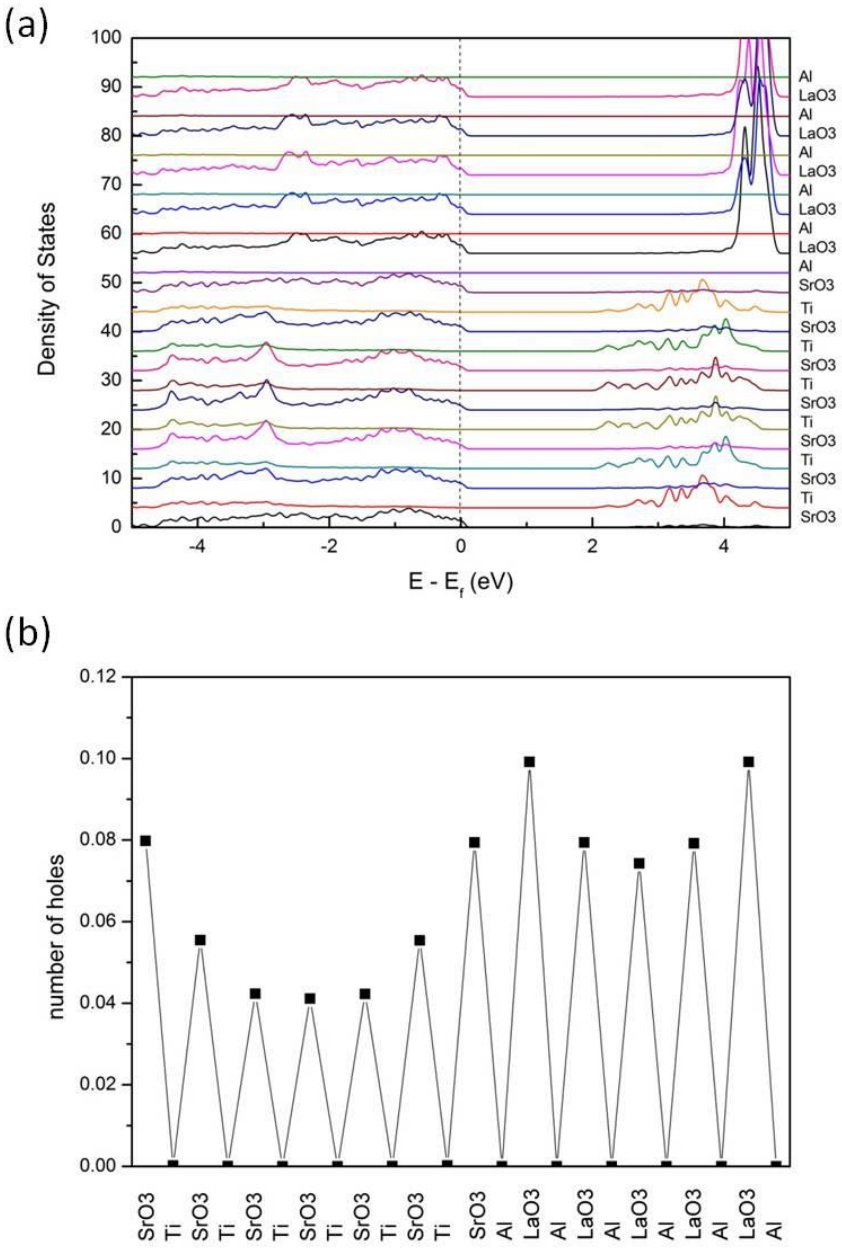

Figure 5-7 (a) Layer-DOS of p-type (111) $(LAO)_6/(STO)_6$ SL, and (b) distribution of holes in p-type SL.

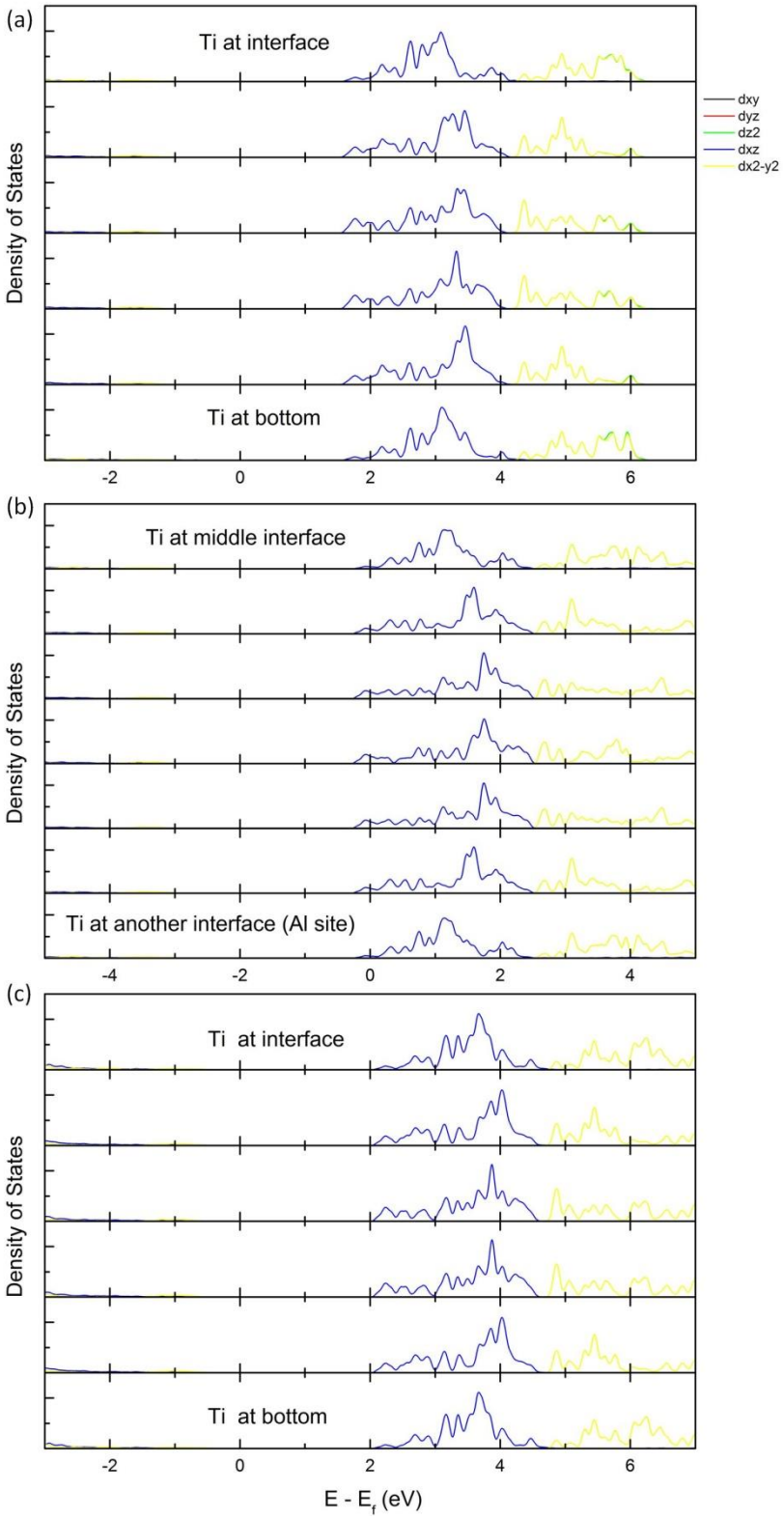

Figure 5-8 Partial Density of States (PDOS) of Ti in (a) intrinsic, (b) n-type doped and (c) p-type doped $(LAO)_6/(STO)_6$ SL. It should be noted that the scale is shifted for Figure5-7 (b).

In Figure 5-8, the PDOS of Ti is shown. One can see that the PDOS of n-type doped (Ti on Al site) SL is similar to that of intrinsic or p-type doped, but all peaks shift in energy correspondingly, since doping may change the chemical potential of electrons. In PDOS of Ti as shown in Figure 5-8, the peaks of the states of Ti d_{xy}, d_{yz} and d_{xz} are completely overlapped, and these orbitals are equivalent under 3-fold symmetry at the (111) interface. Ti d_{xy}, d_{yz} and d_{xz} belong to the t_{2g} orbital. Ti d_{z2} and d_{x2-y2} are the e_g orbital. It can be seen that Ti d orbitals are split into e_g with higher energy and t_{2g} with lower energy as expected in crystal field theory, but e_g state is of less interest because almost no electrons would occupy these high energy orbitals, and it should not affect the conduction. Although d_{xy}, d_{yz} and d_{xz} are overlapped, the t_{2g} orbital may not be degenerated. At both (001) and (111) interfaces of LAO/STO, the t_{2g} orbitals are split, but the degeneracy of t_{2g} is unlike the (001) LAO/STO heterostructure, and it will be shown later in this report. It is interesting to see that the peak of the t_{2g} ($d_{xy,}$ d_{yz} and d_{xz}) states around Fermi-level are depressed at interface. It indicates that the conduction electrons should distribute in STO away from interface, and it is different from the 2DEG at (001) LAO/STO that most of the 2DEG occupy the Ti t_{2g} orbitals at (001) interface.

In Figure 5-9, the band structure of (111) LAO_6/STO_6 SL is illustrated. One can see that the Fermi-level E_f moves to E_{fn} with n-type doping or E_{fp} with p-type doping; while the band gaps remains, but no in-gap states can be found. One can also see that at Γ point, three bands in a set with deviation less than 0.1 eV are located in the region of conduction band. We believe that each set should be contributed by t_{2g} of Ti at different layers in STO. The set of bands with the lowest energy in the conduction band are

contributed by t_{2g} states of Ti located by 3 to 4 monolayers away from both interfaces, and the states of the set of the next lowest energy should be contributed by t_{2g} states of Ti located within about 2 monolayers from interfaces. The three bands in each set have different curvature around Γ point which is similar to the case of (001) LAO/STO with the flat Ti d_{xz} bands along y direction and steeper Ti d_{xy} and d_{yz} bands. It should be noted that our results are in agreement with the analysis of 2-dimensional t_{2g} systems by Chen and Balents [95]. It is suggested that t_{2g} orbitals of (111) interface of systems with structure of STO, are combinations of $d_{xy,}$ d_{yz} and d_{xz} , and t_{2g} further splits into one a_{1g} state and two e'_{2g} states. However, the a_{1g} state and e'_{2g} states cannot be identified from the band diagram, since some states degenerate with the more massive band of lower energy as shown in the lowest set of t_{2g}, but some states degenerate with the lighter band of higher energy as shown in the second lowest set of t_{2g}.

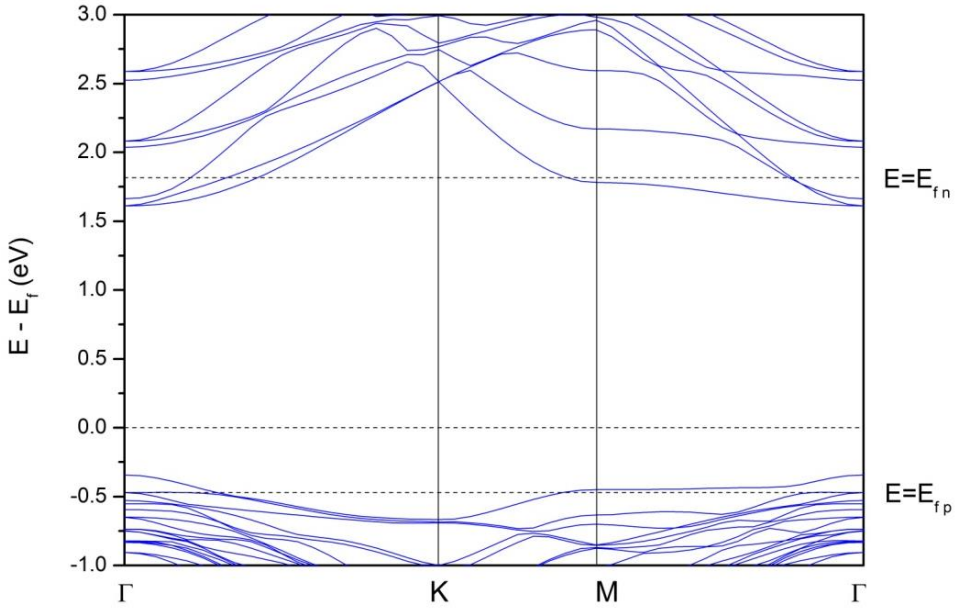

Figure 5-9 Band structure of $(LAO)_6/(STO)_6$ and the plane of first Brillouin zone parallel to (111) interface, with points Γ(0,0), K (-1/3, 1/3) and M(0, 1/2), in terms of reciprocal lattice vectors.

5.3.3 Oxygen Vacancy Effect

Transport properties and electronic structure of (111) LAO/STO SL with oxygen vacancies (OV) are also studied. Distribution of electrons in the SL with OV at n-type and p-type interfaces in LAO, which are denoted by V_n (at the LaO_3 layer of $LaO_3/Ti/SrO_3$) and V_p (at the LaO_3 layer of $LaO_3/Al/SrO_3$), were calculated. In the SL, two extra electrons are provided by an OV in the LAO/STO SL. In Figure 5-10, the distributions of electrons in the SL with OV at n-type and p-type interfaces are illustrated. For the SL with OV at V_n, most electrons are located around the OV, and some electrons spread to the SrTiO layers in STO. For the SL with OV at V_p, however, most electrons spread to the SrTiO layers in STO. The distribution of the electrons is similar to the OV at (001) LAO/STO SL[98]. No matter at which site OV locate, the distribution of electrons in STO away from OV is similar to those of n-type doped SL in Figure 4-4 (b), and it depends little on the location of OV. This suggests that some extra electrons are localized around the site of oxygen vacancy (OV), while some are spreading in STO as n-type dopant.

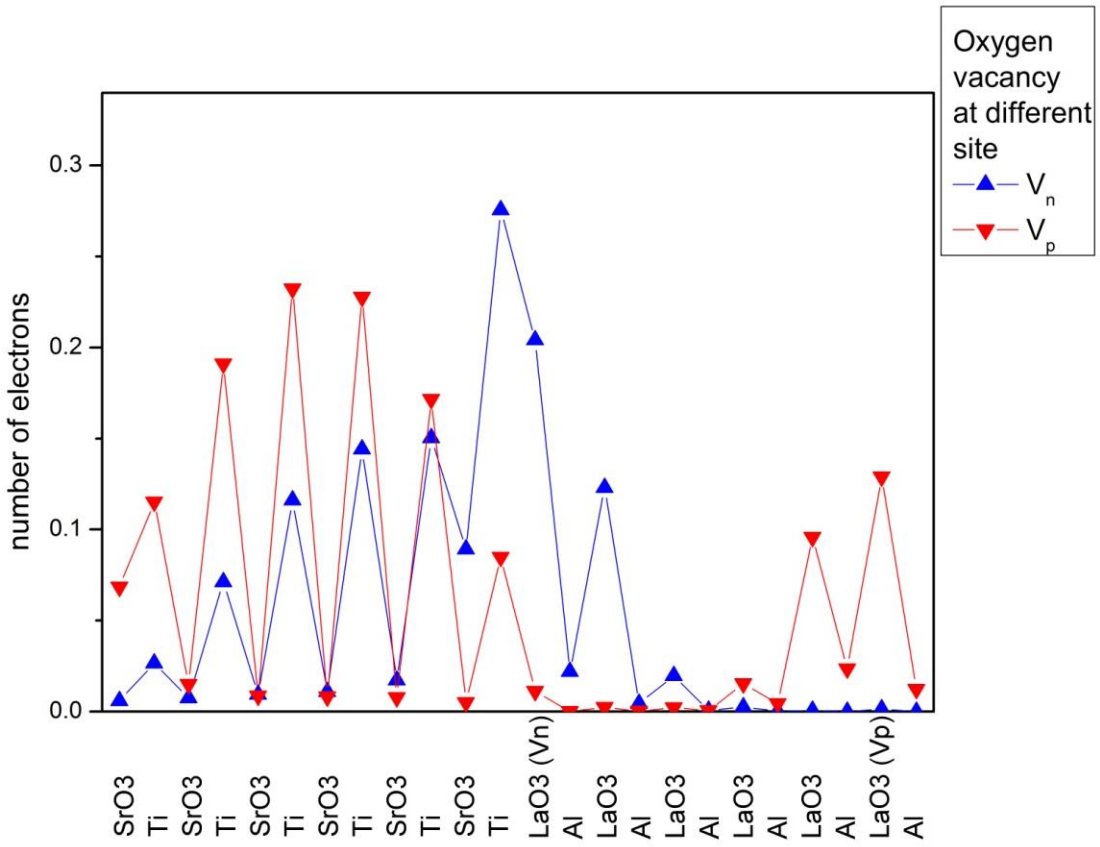

Figure 5-10 Distribution of electrons in SL with OV at n-type and p-type interfaces.

Band structures with OV at site V_n is shown in Figure 5-11 and similar results have also been observed with OV at the site V_p. With the presence of oxygen vacancy (OV) in STO or LAO, an additional band appears below the bottom of conduction band. The additional state with oxygen vacancy has also been reported in theoretical studies of the bulk and (001) surface of $SrTiO_3$ [96, 97] and (001) interface of $LaAlO_3/SrTiO_3$[98]. This state is partially contributed by the e_g orbitals for the systems with OV at V_n. It should be noticed that the density of OV in our calculation is very high (1 OV per 1×1 unit), and the band due to OV should be more localized at lower density of OV as shown in ref. [97]. Therefore, the conductivity should be contributed by the t_{2g} orbitals as in the n-type doped LAO/STO.

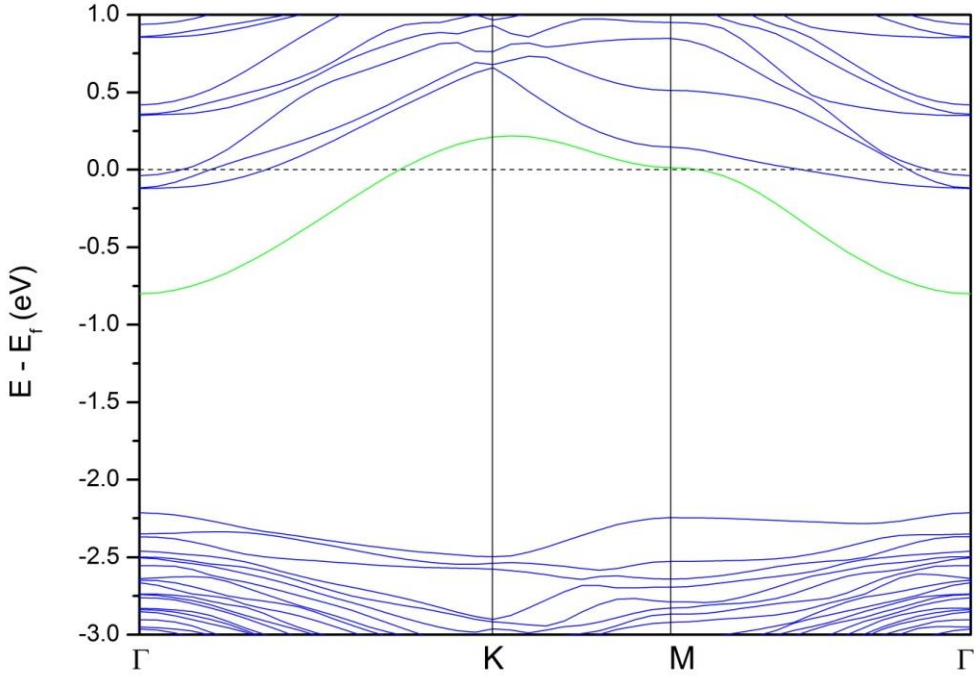

Figure 5-11 Band structure of SL with OV at site V_n, the extra band is in green.

2DEG at (001) LAO/STO is believed to be driven by the polar discontinuity at the interface. The conduction electrons are contributed by three components of reconstructed Ti d orbitals, most at Ti d_{xy} and a little at Ti d_{yz}/d_{xz}. The first one is lower in energy and strongly confined within several layers of STO from interface, but the second one should distribute deeper in STO.

In comparison to (001) LAO/STO, the conduction state is less likely to occur due to polar catastrophe at (111) LAO/STO. The t_{2g} orbitals at (111) LAO/STO is different. It does not split as much as those at (001) LAO/STO. The energy of the more massive band of t_{2g} is not higher than the energy of the other two t_{2g} bands as shown in Figure 5-9. It can be expected that the 2DEG at (111) LAO/STO, if it exists or be

produced by doping or oxygen vacancy, would be more localized than those at (001) LAO/STO.

5.4 Conclusion

In conclusion, we have investigated the electronic properties of (111) LAO/STO interface. It is unexpected that the effect of polar discontinuity is fully cancelled. The conduction at (111) LAO/STO interface, if obtained due to doping or other sources, should be contributed by Ti t_{2g} orbitals which also contribute to the 2DEG at (001) LAO/STO. The distribution and the transport properties of the conduction electrons should be different from those at (001) LAO/STO heterostructure.

CHAPTER 6 CONCLUSION AND FUTURE WORK

6.1 Conclusion

In this thesis, the $LaAlO_3/SrTiO_3$ heterostructure and related systems have been investigated by first-principles calculation in the frame of Density Functional Theory. The phenomenon of the transport properties at the LAO/STO interface influenced by adsorbate of polar molecules has been studied in a specified case of H_2O. The mechanisms of conduction at (110) and (111) LAO/STO heterostructures have also been studied. The main results of this thesis are listed.

(1) Properties, mainly the electronic properties, of the $LaAlO_3/SrTiO_3$ heterostructures, including (001) LAO/STO with or without H_2O mulecules, (110) and (111) LAO/STO heterostructures, have been determined.

(2) H_2O, as a polar molecule, increases the carrier density of 2DEG at LAO/STO interface. Calculation suggests that the surface state is varied to transfer more electrons to interface for a monolayer of water molecules on surface. For more water molecules, water molecules may provide a certain amount of electrons to the interface of LAO/STO.

(3) Different to (001) LAO/STO, stoichiometric (110) LAO/STO interface should remain insulating.

(4) The conduction at (110) LAO/STO heterostructure, if conduction electrons present due to doping, is different from the 2DEG at (001) LAO/STO interface. The main difference is its anisotropic transport along different in-plane directions. Another difference is the distribution of conduction electrons in STO. The 2DEG at (001) LAO/STO is strongly confined to the TiO_2 layer next to LAO, but the conduction electrons at (110) LAO/STO tend to spread away from the interface.

(5) Stoichiometric (111) LAO/STO heterostructure may remain insulating. At the (111) LAO/STO interface, polar discontinuity is expected due to the charge at ionic limit of LAO and STO. But the electric field due to polar discontinuity may be cancelled by the field due to atomic relaxation.

(6) Similar to the (110) LAO/STO, conduction electrons at (111) LAO/STO heterostructure can be induced by doping like oxygen vacancies. Conduction electrons at (111) LAO/STO interface locate at Ti away from the interfaces. These electrons may also be “heavier” to transport than those at (001) LAO/STO.

Because of limitations in computational capacity, some improvements can be made in future.

6.2 Future Work

For the model with the amount of H_2O more than a monolayer in Chapter 3, it would be better to apply simulation of ab initio Molecular Dynamics to test the stability. Actually, ab initio Molecular Dynamics calculation was tried, but it is too demanding for our computers.

The effects of oxygen vacancy at (110) and (111) LAO/STO are calculated in the supercell of (1×1) interface unit cell. The density should be too high to occur. Also, it may be too periodic for the H_2O molecules on (1×1) surface unit cell of LAO/STO. It is better to increase the size of supercell from (1×1) to larger cell like (2×2).

The models of superlattices of LAO/STO at (110) and (111) are built to simulate the properties of these interfaces. The model of thin film (vacuum above LAO, like those in Chapter 3) is closer to the systems tested in experiment. A reason for the choice of the superlattice model, but not the thin film model, like those in Chapter 3, is the lack of the knowledge of the structures of (110) and (111) surfaces of STO and LAO especially. For (001) oriented STO, it consists of two neutral layers SrO and TiO_2, and (001) LAO consists of two layers (LaO^+ and AlO_2^-) with +/-1 e charge per 1×1 surface unit cell. However, for the (110) or (111) oriented thin films, they consist of layers with charges equal to +/-3e or +/-4e. As the (110) and (111) layers are highly charged, strong polar discontinuity occurs between the film and vacuum. If the atom remains in the order of bulk, the structure should become unstable. The structure of (110) and (111) surfaces should be therefore different from the bulk structure. However, we know little

about (110) and (111) surface of LAO and STO. For example, we do not know if surface reconstruction occurs at the upper and lower surface or not. In this work, we simply ignored the surface effect in superlattice model. Therefore, (110) and (111) LAO/STO should be studied by first principles in thin film model, but first the structure of these surfaces should be studied first by simulations or experiments.

After the study of thin film models of (110) and (111) LAO/STO, modification of their surface may be studied to show whether the phenomenon due to polar molecules at (001) LAO/STO occurs similarly or not. For example, it is interesting to study the impact of H_2O adsorption on the conduction of (011) and (111) LAO/STO.

REFERENCES

[1] A. Ohtomo and H. Y. Hwang, "A high-mobility electron gas at the LaAlO3/SrTiO3 heterointerface," *Nature*, vol. 427, pp. 423-426, 2004.

[2] C. Cen, S. Thiel, G. Hammerl, C. W. Schneider, K. E. Andersen, C. S. Hellberg, J. Mannhart, and J. Levy, "Nanoscale control of an interfacial metal-insulator transition at room temperature," *Nature Mater.*, vol. 7, pp. 298-302, 2008.

[3] A. D. Caviglia, S. Gariglio, N. Reyren, D. Jaccard, T. Schneider, M. Gabay, S. Thiel, G. Hammerl, J. Mannhart, and J. M. Triscone, "Electric field control of the LaAlO3/SrTiO3 interface ground state," *Nature*, vol. 456, pp. 624-627, 2008.

[4] N. Reyren, M. Bibes, E. Lesne, J. M. George, C. Deranlot, S. Collin, A. Barthélémy, and H. Jaffrès, "Gate-Controlled Spin Injection at LaAlO3/SrTiO3 Interfaces," *Phys. Rev. Lett.*, vol. 108, p. 186802, 2012.

[5] F. Gunkel, P. Brinks, S. Hoffmann-Eifert, R. Dittmann, M. Huijben, J. E. Kleibeuker, G. Koster, G. Rijnders, and R. Waser, "Influence of charge compensation mechanisms on the sheet electron density at conducting LaAlO3/SrTiO3-interfaces," *Appl. Phys. Lett.*, vol. 100, pp. 052103-3, 2012.

[6] M. Huijben, A. Brinkman, G. Koster, G. Rijnders, H. Hilgenkamp, and D. H. A. Blank, "Structure–Property Relation of SrTiO3/LaAlO3 Interfaces," *Adv. Mater.*, vol. 21, pp. 1665-1677, 2009.

[7] H. Chen, A. M. Kolpak, and S. Ismail-Beigi, "Electronic and Magnetic Properties of SrTiO3/LaAlO3 Interfaces from First Principles," *Adv. Mater.*, vol. 22, pp. 2881-2899, 2010.

[8] J. Mannhart and D. G. Schlom, "Oxide Interfaces—An Opportunity for Electronics," *Science*, vol. 327, pp. 1607-1611, March, 2010.

[9] S. A. Chambers, "Understanding the mechanism of conductivity at the LaAlO3/SrTiO3(001) interface," *Surf. Sci.*, vol. 605, pp. 1133-1140, 2011.

[10] N. Pavlenko, T. Kopp, E. Y. Tsymbal, J. Mannhart, and G. A. Sawatzky, "Oxygen vacancies at titanate interfaces: Two-dimensional magnetism and orbital reconstruction," *Phys. Rev. B*, vol. 86, p. 064431, 2012.

[11] N. Pavlenko, T. Kopp, E. Y. Tsymbal, G. A. Sawatzky, and J. Mannhart, "Magnetic and superconducting phases at the LaAlO3/SrTiO3 interface: The role of interfacial Ti 3d electrons," *Phys. Rev. B*, vol. 85, p. 020407, 2012.

[12] N. Reyren, S. Thiel, A. D. Caviglia, L. F. Kourkoutis, G. Hammerl, C. Richter, C.

W. Schneider, T. Kopp, A.-S. Rüetschi, D. Jaccard, M. Gabay, D. A. Muller, J.-M. Triscone, and J. Mannhart, "Superconducting Interfaces Between Insulating Oxides," *Science*, vol. 317, pp. 1196-1199, August, 2007.

[13] K. Michaeli, A. C. Potter, and P. A. Lee, "Superconducting and Ferromagnetic Phases in SrTiO3/LaAlO3 Oxide Interface Structures: Possibility of Finite Momentum Pairing," *Phys. Rev. Lett.*, vol. 108, p. 117003, 2012.

[14] S. Seri, M. Schultz, and L. Klein, "Interplay between sheet resistance increase and magnetotransport properties in LaAlO3/SrTiO3," *Physical Review B*, vol. 86, p. 085118, 2012.

[15] D. A. Dikin, M. Mehta, C. W. Bark, C. M. Folkman, C. B. Eom, and V. Chandrasekhar, "Coexistence of Superconductivity and Ferromagnetism in Two Dimensions," *Phys. Rev. Lett.*, vol. 107, p. 056802, 2011.

[16] Y. Xie, C. Bell, T. Yajima, Y. Hikita, and H. Y. Hwang, "Charge Writing at the LaAlO3/SrTiO3 Surface," *Nano Lett.*, vol. 10, pp. 2588-2591, 2010.

[17] C. W. Bark, P. Sharma, Y. Wang, S. H. Baek, S. Lee, S. Ryu, C. M. Folkman, T. R. Paudel, A. Kumar, S. V. Kalinin, A. Sokolov, E. Y. Tsymbal, M. S. Rzchowski, A. Gruverman, and C. B. Eom, "Switchable Induced Polarization in LaAlO3/SrTiO3 Heterostructures," *Nano Lett.*, vol. 12, pp. 1765-1771, 2012.

[18] R. Pentcheva, M. Huijben, K. Otte, W. E. Pickett, J. E. Kleibeuker, J. Huijben, H. Boschker, D. Kockmann, W. Siemons, G. Koster, H. J. W. Zandvliet, G. Rijnders, D. H. A. Blank, H. Hilgenkamp, and A. Brinkman, "Parallel Electron-Hole Bilayer Conductivity from Electronic Interface Reconstruction," *Phys. Rev. Lett.*, vol. 104, p. 166804, 2010.

[19] M. Huijben, D. Kockmann, J. Huijben, J. E. Kleibeuker, A. van Houselt, G. Koster, D. H. A. Blank, H. Hilgenkamp, G. Rijnders, A. Brinkman, and H. J. W. Zandvliet, "Local probing of coupled interfaces between two-dimensional electron and hole gases in oxide heterostructures by variable-temperature scanning tunneling spectroscopy," *Phys. Rev. B*, vol. 86, p. 035140, 2012.

[20] F. Bi, D. F. Bogorin, C. Cen, C. W. Bark, J.-W. Park, C.-B. Eom, and J. Levy, "``Water-cycle" mechanism for writing and erasing nanostructures at the LaAlO3/SrTiO3 interface," *Appl. Phys. Lett.*, vol. 97, pp. 173110-3, 2010.

[21] Y. Xie, Y. Hikita, C. Bell, and H. Y. Hwang, "Control of electronic conduction at an oxide heterointerface using surface polar adsorbates," *Nature Commun.*, vol. 2, p. 494, 2011.

[22] K. Au, D. F. Li, N. Y. Chan, and J. Y. Dai, "Polar Liquid Molecule Induced Transport Property Modulation at LaAlO3/SrTiO3 Heterointerface," *Adv. Mater.*,

vol. 24, pp. 2598-2602, 2012.

[23] S. Won-joon, C. Eunae, L. Jaichan, and H. Seungwu, "Hydrogen adsorption and carrier generation in LaAlO 3 –SrTiO 3 heterointerfaces: a first-principles study," *J. Phys.: Condens. Matter,* vol. 22, p. 315501, 2010.

[24] D. V. Christensen, F. Trier, Y. Z. Chen, A. Smith, J. Nygard, and N. Pryds, "Controlling interfacial states in amorphous/crystalline LaAlO[sub 3]/SrTiO[sub 3] heterostructures by electric fields," *Appl. Phys. Lett.,* vol. 102, pp. 021602-4, 2013.

[25] G. Herranz, F. Sánchez, N. Dix, M. Scigaj, and J. Fontcuberta, "High mobility conduction at (110) and (111) LaAlO3/SrTiO3 interfaces," *Sci. Rep.,* vol. 2, 2012.

[26] W. A. Harrison, E. A. Kraut, J. R. Waldrop, and R. W. Grant, "Polar heterojunction interfaces," *Phys. Rev. B,* vol. 18, pp. 4402-4410, 1978.

[27] Z. Schlesinger, J. C. M. Hwang, and S. J. Allen, Jr., "Subband-Landau-Level Coupling in a Two-Dimensional Electron Gas," *Phys. Rev. Lett.,* vol. 50, pp. 2098-2101, 1983.

[28] H. L. Störmer, R. Dingle, A. C. Gossard, W. Wiegmann, and M. D. Sturge, "Two-dimensional electron gas at a semiconductor-semiconductor interface," *Solid State Commun.,* vol. 29, pp. 705-709, 1979.

[29] M. Brandt, H. von Wenckstern, G. Benndorf, H. Hochmuth, M. Lorenz, and M. Grundmann, "Formation of a two-dimensional electron gas in ZnO/MgZnO single heterostructures and quantum wells," *Thin Solid Films,* vol. 518, pp. 1048-1052, 2009.

[30] D. Spirito, L. Di Gaspare, F. Evangelisti, A. Di Gaspare, E. Giovine, and A. Notargiacomo, "Weak antilocalization and spin-orbit interaction in a two-dimensional electron gas," *Phys. Rev. B,* vol. 85, p. 235314, 2012.

[31] M. Breitschaft, V. Tinkl, N. Pavlenko, S. Paetel, C. Richter, J. R. Kirtley, Y. C. Liao, G. Hammerl, V. Eyert, T. Kopp, and J. Mannhart, "Two-dimensional electron liquid state at LaAlO3-SrTiO3 interfaces," *Phys. Rev. B,* vol. 81, p. 153414, 2010.

[32] A. Dubroka, M. Rössle, K. W. Kim, V. K. Malik, L. Schultz, S. Thiel, C. W. Schneider, J. Mannhart, G. Herranz, O. Copie, M. Bibes, A. Barthélémy, and C. Bernhard, "Dynamical Response and Confinement of the Electrons at the LaAlO3/SrTiO3 Interface," *Phys. Rev. Lett.,* vol. 104, p. 156807, 2010.

[33] V. Tinkl, M. Breitschaft, C. Richter, and J. Mannhart, "Large negative electronic compressibility of LaAlO3-SrTiO3 interfaces with ultrathin LaAlO3 layers,"

Phys. Rev. B, vol. 86, p. 075116, 2012.

[34] T. Yamamoto and T. Mizoguchi, "Defect energetics in LaAlO3 polymorphs: A first-principles study," *Phys. Rev. B,* vol. 86, p. 094117, 2012.

[35] A. A. Knizhnik, I. M. Iskandarova, A. A. Bagatur'yants, B. V. Potapkin, L. R. C. Fonseca, and A. Korkin, "First-principles calculations of the electrical properties of LaAlO3 and its interface with Si," *Phys. Rev. B,* vol. 72, p. 235329, 2005.

[36] W. Zhong, D. Vanderbilt, and K. M. Rabe, "Phase Transitions in BaTiO3 from First Principles," *Phys. Rev. Lett.*, vol. 73, pp. 1861-1864, 1994.

[37] E. Heifets, E. Kotomin, and V. A. Trepakov, "Calculations for antiferrodistortive phase of SrTiO 3 perovskite: hybrid density functional study," *J. Phys.: Condens. Matter,* vol. 18, p. 4845, 2006.

[38] N. Sai and D. Vanderbilt, "First-principles study of ferroelectric and antiferrodistortive instabilities in tetragonal SrTiO3," *Phys. Rev. B,* vol. 62, pp. 13942-13950, 2000.

[39] W. Luo, W. Duan, S. G. Louie, and M. L. Cohen, "Structural and electronic properties of n-doped and p-doped SrTiO3," *Phys. Rev. B,* vol. 70, p. 214109, 2004.

[40] M. Jourdan, N. Blümer, and H. Adrian, "Superconductivity of SrTiO," *Eur. Phys. J. B,* vol. 33, pp. 25-30, 2003.

[41] A. Sorokine, D. Bocharov, S. Piskunov, and V. Kashcheyevs, "Electronic charge redistribution in LaAlO3(001) thin films deposited at SrTiO3(001) substrate: First-principles analysis and the role of stoichiometry," *Phys. Rev. B,* vol. 86, p. 155410, 2012.

[42] J. Verbeeck, S. Bals, A. N. Kravtsova, D. Lamoen, M. Luysberg, M. Huijben, G. Rijnders, A. Brinkman, H. Hilgenkamp, D. H. A. Blank, and G. Van Tendeloo, "Electronic reconstruction at n-type SrTiO3/LaAlO3 interfaces," *Phys. Rev. B,* vol. 81, p. 085113, 2010.

[43] Z. Zhicheng and J. K. Paul, "Electronic-structure–induced reconstruction and magnetic ordering at the LaAlO 3 |SrTiO 3 interface," *Europhys. Lett.*, vol. 84, p. 27001, 2008.

[44] M. Stengel, "First-Principles Modeling of Electrostatically Doped Perovskite Systems," *Phys. Rev. Lett.*, vol. 106, p. 136803, 2011.

[45] H. Chen, A. Kolpak, and S. Ismail-Beigi, "First-principles study of electronic reconstructions of LaAlO3/SrTiO3 heterointerfaces and their variants," *Phys. Rev. B,* vol. 82, p. 085430, 2010.

[46] X. Yang and H. Su, "Polarization and Electric Field Dependence of Electronic

Properties in LaAlO3/SrTiO3 Heterostructures," *ACS Appl. Mater. Interfaces*, vol. 3, pp. 3819-3823, 2011.

[47] J. Lee and A. A. Demkov, "Charge origin and localization at the n-type SrTiO3/LaAlO3 interface," *Phys. Rev. B*, vol. 78, p. 193104, 2008.

[48] P. R. Willmott, S. A. Pauli, R. Herger, C. M. Schlepütz, D. Martoccia, B. D. Patterson, B. Delley, R. Clarke, D. Kumah, C. Cionca, and Y. Yacoby, "Structural Basis for the Conducting Interface between LaAlO3 and SrTiO3," *Phys. Rev. Lett.*, vol. 99, p. 155502, 2007.

[49] M. S. Park, S. H. Rhim, and A. J. Freeman, "Charge compensation and mixed valency in LaAlO3/SrTiO3 heterointerfaces studied by the FLAPW method," *Phys. Rev. B*, vol. 74, p. 205416, 2006.

[50] S. Thiel, G. Hammerl, A. Schmehl, C. W. Schneider, and J. Mannhart, "Tunable Quasi-Two-Dimensional Electron Gases in Oxide Heterostructures," *Science*, vol. 313, pp. 1942-1945, September, 2006.

[51] S. Nazir, N. Singh, and U. Schwingenschlögl, "Charge transfer mechanism for the formation of metallic states at the KTaO3/SrTiO3 interface," *Phys. Rev. B*, vol. 83, p. 113107, 2011.

[52] A. Kalabukhov, R. Gunnarsson, T. Claeson, and D. Winkler, "Electrical transport properties of polar heterointerface between KTaO3 and SrTiO3," *preprint at* http://arxiv.org/abs/0704.1050v1.

[53] J. Biscaras, N. Bergeal, S. Hurand, C. Grossetête, A. Rastogi, R. C. Budhani, D. LeBoeuf, C. Proust, and J. Lesueur, "Two-Dimensional Superconducting Phase in LaTiO3/SrTiO3 Heterostructures Induced by High-Mobility Carrier Doping," *Phys. Rev. Lett.*, vol. 108, p. 247004, 2012.

[54] K. Rahmanizadeh, G. Bihlmayer, M. Luysberg, and S. Blügel, "First-principles study of intermixing and polarization at the DyScO3/SrTiO3 interface," *Phys. Rev. B*, vol. 85, p. 075314, 2012.

[55] Z. Zhicheng, W. Philipp, H. Karsten, and S. Giorgio, "Microscopic understanding of the orbital splitting and its tuning at oxide interfaces," *Europhys. Lett.*, vol. 99, p. 37011, 2012.

[56] V. R. Cooper, "Enhanced carrier mobilities in two-dimensional electron gases at III-III/I-V oxide heterostructure interfaces," *Phys. Rev. B*, vol. 85, p. 235109, 2012.

[57] S. C. Chae, W. S. Choi, H. K. Yoo, and B. S. Kang, "Metal-Insulator-like transition in the LaAlO3/BaTiO3 interface," *Curr. Appl. Phys.*, vol. 11, pp. 521-524, 2011.

[58] Y. Wang, M. K. Niranjan, K. Janicka, J. P. Velev, M. Y. Zhuravlev, S. S. Jaswal, and E. Y. Tsymbal, "Ferroelectric dead layer driven by a polar interface," *Phys. Rev. B,* vol. 82, p. 094114, 2010.

[59] J. Shen, H. Lee, R. Valentí, and H. O. Jeschke, "Ab initio study of the two-dimensional metallic state at the surface of SrTiO3: Importance of oxygen vacancies," *Phys. Rev. B,* vol. 86, p. 195119, 2012.

[60] W. Meevasana, P. D. C. King, R. H. He, S. K. Mo, M. Hashimoto, A. Tamai, P. Songsiriritthigul, F. Baumberger, and Z. X. Shen, "Creation and control of a two-dimensional electron liquid at the bare SrTiO3 surface," *Nature Mater.,* vol. 10, pp. 114-118, 2011.

[61] H. Gross, N. Bansal, Y.-S. Kim, and S. Oh, "In situ study of emerging metallicity on ion-bombarded SrTiO3 surface," *J. Appl. Phys.,* vol. 110, pp. 073704-6, 2011.

[62] G. Khalsa and A. H. MacDonald, "Theory of the SrTiO3 surface state two-dimensional electron gas," *Phys. Rev. B,* vol. 86, p. 125121, 2012.

[63] A. F. Santander-Syro, O. Copie, T. Kondo, F. Fortuna, S. Pailhes, R. Weht, X. G. Qiu, F. Bertran, A. Nicolaou, A. Taleb-Ibrahimi, P. Le Fevre, G. Herranz, M. Bibes, N. Reyren, Y. Apertet, P. Lecoeur, A. Barthelemy, and M. J. Rozenberg, "Two-dimensional electron gas with universal subbands at the surface of SrTiO3," *Nature,* vol. 469, pp. 189-193, 2011.

[64] Y. F. Zhukovskii, E. A. Kotomin, S. Piskunov, and D. E. Ellis, "A comparative ab initio study of bulk and surface oxygen vacancies in PbTiO3, PbZrO3 and SrTiO3 perovskites," *Solid State Commun.,* vol. 149, pp. 1359-1362, 2009.

[65] Y. Chen, N. Pryds, J. e. E. Kleibeuker, G. Koster, J. Sun, E. Stamate, B. Shen, G. Rijnders, and S. Linderoth, "Metallic and Insulating Interfaces of Amorphous SrTiO3-Based Oxide Heterostructures," *Nano Lett.,* vol. 11, pp. 3774-3778, 2011.

[66] P. Brinks, W. Siemons, J. E. Kleibeuker, G. Koster, G. Rijnders, and M. Huijben, "Anisotropic electrical transport properties of a two-dimensional electron gas at SrTiO3--LaAlO3 interfaces," *Appl. Phys. Lett.,* vol. 98, pp. 242904-3, 2011.

[67] T. Fix, F. Schoofs, Z. Bi, A. Chen, H. Wang, J. L. MacManus-Driscoll, and M. G. Blamire, "Influence of SrTiO3 substrate miscut angle on the transport properties of LaAlO3/SrTiO3 interfaces," *Appl. Phys. Lett.,* vol. 99, pp. 022103-3, 2011.

[68] N. C. Bristowe, T. Fix, M. G. Blamire, P. B. Littlewood, and E. Artacho, "Proposal of a One-Dimensional Electron Gas in the Steps at the LaAlO3-SrTiO3 Interface," *Phys. Rev. Lett.,* vol. 108, p. 166802, 2012.

[69] R. Arras, V. G. Ruiz, W. E. Pickett, and R. Pentcheva, "Tuning the two-dimensional electron gas at the LaAlO3/SrTiO3(001) interface by metallic contacts," *Phys. Rev. B,* vol. 85, p. 125404, 2012.

[70] C. Cazorla and M. Stengel, "First-principles modeling of Pt/LaAlO3/SrTiO3 capacitors under an external bias potential," *Phys. Rev. B,* vol. 85, p. 075426, 2012.

[71] G. Kresse and J. Furthmüller, "Efficient iterative schemes for ab initio total-energy calculations using a plane-wave basis set," *Phys. Rev. B,* vol. 54, pp. 11169-11186, 1996.

[72] G. Kresse and J. Furthmüller, "Efficiency of ab-initio total energy calculations for metals and semiconductors using a plane-wave basis set," *Comput. Mater. Sci.,* vol. 6, pp. 15-50, 1996.

[73] K. Ohno, K. Esfarjani, and Y. Kawazoe, "Ab Initio Methods," in *Comput. Mater. Sci.*. vol. 129, ed: Springer Berlin Heidelberg, 1999, pp. 7-138.

[74] R. M. Martin, *Electronic Structure: Basic Theory and Practical Methods*: Cambridge University Press, 2004.

[75] N. M. Harrison, "An Introduction to Density Functional Theory," in *Computational Materials Science*, C. R. A. Catlow, IOS Press, 2003.

[76] R. O. Jones and O. Gunnarsson, "The density functional formalism, its applications and prospects," *Rev. of Mod. Phys.,* vol. 61, pp. 689-746, 1989.

[77] A. J. Freeman and E. Wimmer, "Density Functional Theory as a Major Tool in Computational Materials Science," *Ann. Review of Mater. Sci.,* vol. 25, pp. 7-36, 1995.

[78] A. V. Postnikov, "Methods of electronic structure calculations," in *Computational Materials Science*, C. R. A. Catlow, IOS Press, 2003.

[79] P. E. Blöchl, "Projector augmented-wave method," *Phys. Rev. B,* vol. 50, pp. 17953-17979, 1994.

[80] G. Kresse and D. Joubert, "From ultrasoft pseudopotentials to the projector augmented-wave method," *Phys. Rev. B,* vol. 59, pp. 1758-1775, 1999.

[81] H. J. Monkhorst and J. D. Pack, "Special points for Brillouin-zone integrations," *Phys. Rev. B,* vol. 13, pp. 5188-5192, 1976.

[82] J. Neugebauer and M. Scheffler, "Adsorbate-substrate and adsorbate-adsorbate interactions of Na and K adlayers on Al(111)," *Phys. Rev. B,* vol. 46, pp. 16067-16080, 1992.

[83] G. Makov and M. C. Payne, "Periodic boundary conditions in ab initio calculations," *Phys. Rev. B,* vol. 51, pp. 4014-4022, 1995.

[84] M. Dawber, K. M. Rabe, and J. F. Scott, "Physics of thin-film ferroelectric oxides," *Rev. Mod. Phys.*, vol. 77, pp. 1083-1130, 2005.

[85] B. Meyer and D. Vanderbilt, "Ab initio study of BaTiO3 and PbTiO3 surfaces in external electric fields," *Phys. Rev. B,* vol. 63, p. 205426, 2001.

[86] C. Cen, S. Thiel, J. Mannhart, and J. Levy, "Oxide Nanoelectronics on Demand," *Science,* vol. 323, pp. 1026-1030, February, 2009.

[87] Y. Xie, C. Bell, Y. Hikita, and H. Y. Hwang, "Tuning the Electron Gas at an Oxide Heterointerface via Free Surface Charges," *Adv Mater.,* vol. 23, pp. 1744-1747, 2011.

[88] G. Geneste and B. Dkhil, "Adsorption and dissociation of H2O on in-plane-polarized BaTiO3(001) surfaces and their relation to ferroelectricity," *Phys. Rev. B,* vol. 79, p. 235420, 2009.

[89] R. A. Evarestov, A. V. Bandura, and V. E. Alexandrov, "Adsorption of water on surface of SrTiO3 and SrZrO3 cubic perovskites: Hybrid HF-DFT LCAO calculations," *Surf. Sci.*, vol. 601, pp. 1844-1856, 2007.

[90] J. A. Snyder, D. R. Alfonso, J. E. Jaffe, Z. Lin, A. C. Hess, and M. Gutowski, "Periodic Density Functional LDA and GGA Study of CO Adsorption at the (001) Surface of MgO," *J. Phys. Chem. B,* vol. 104, pp. 4717-4722, 2000.

[91] S. Fahy, X. W. Wang, and S. G. Louie, "Variational Quantum Monte Carlo Nonlocal Pseudopotential Approach to Solids: Cohesive and Structural Properties of Diamond," *Phys. Rev. Lett.*, vol. 61, pp. 1631-1634, 1988.

[92] W.-j. Son, E. Cho, B. Lee, J. Lee, and S. Han, "Density and spatial distribution of charge carriers in the intrinsic n-type LaAlO3-SrTiO3 interface," *Phys. Rev. B,* vol. 79, p. 245411, 2009.

[93] H. Chen, A. M. Kolpak, and S. Ismail-Beigi, "Fundamental asymmetry in interfacial electronic reconstruction between insulating oxides: An ab initio study," *Phys. Rev. B,* vol. 79, p. 161402, 2009.

[94] O. Copie, V. Garcia, C. Bödefeld, C. Carrétéro, M. Bibes, G. Herranz, E. Jacquet, J. L. Maurice, B. Vinter, S. Fusil, K. Bouzehouane, H. Jaffrès, and A. Barthélémy, "Towards Two-Dimensional Metallic Behavior at LaAlO3/SrTiO3 Interfaces," *Phys. Rev. Lett.*, vol. 102, p. 216804, 2009.

[95] G. Chen and L. Balents, "Ferromagnetism in Itinerant Two-Dimensional t2g Systems," *Phys. Rev. Letters,* vol. 110, p. 206401, 2013.

[96] C. Lin, C. Mitra, and A. A. Demkov, "Orbital ordering under reduced symmetry in transition metal perovskites: Oxygen vacancy in SrTiO3," *Phys. Rev. B,* vol. 86, p. 161102, 2012.

[97] J. Carrasco, F. Illas, N. Lopez, E. A. Kotomin, Y. F. Zhukovskii, R. A. Evarestov, Y. A. Mastrikov, S. Piskunov, and J. Maier, "First-principles calculations of the atomic and electronic structure of F centers in the bulk and on the (001) surface of SrTiO3," *Phys. Rev. B,* vol. 73, p. 064106, 2006.

[98] P. V. Ong and J. Lee, "Orbital-selective charge transfer at oxygen-deficient LaAlO3/SrTiO3(001) interfaces," *Phys. Rev. B,* vol. 87, p. 195212, 2013.

[99] A. Annadi, Q. Zhang, X. Renshaw Wang, N. Tuzla, K. Gopinadhan, W. M. Lü, A. Roy Barman, Z. Q. Liu, A. Srivastava, S. Saha, Y. L. Zhao, S. W. Zeng, S. Dhar, E. Olsson, B. Gu, S. Yunoki, S. Maekawa, H. Hilgenkamp, T. Venkatesan, and Ariando, "Anisotropic two-dimensional electron gas at the LaAlO3/SrTiO3 (110) interface," *Nature Commun.,* vol. 4, p. 1838, 2013.

[100] J. Chang, Y.-S. Park, and S.-K. Kim, "Atomically flat single-terminated SrTiO3 (111) surface," *Appl. Phys. Lett.,* vol. 92, pp. 152910-3, 2008.

[101] J. L. Blok, X. Wan, G. Koster, D. H. A. Blank, and G. Rijnders, "Epitaxial oxide growth on polar (111) surfaces," *Appl. Phys. Lett.,* vol. 99, pp. 151917-3, 2011.

[102] J. M. Albina, M. Mrovec, B. Meyer, and C. Elsässer, "Structure, stability, and electronic properties of SrTiO3⁄LaAlO3 and SrTiO3⁄SrRuO3 interfaces," *Phys. Rev. B,* vol. 76, p. 165103, 2007.

[103] P. Delugas, V. Fiorentini, and A. Filippetti, "Dielectric properties and long-wavelength optical modes of the high-κ oxide LaAlO3," *Phys. Rev. B,* vol. 71, p. 134302, 2005.[104] W. Zhong, R. D. King-Smith, and D. Vanderbilt, "Giant LO-TO splittings in perovskite ferroelectrics," *Phys. Rev. Lett.,* vol. 72, pp. 3618-3621, 1994.